


Review of magnesium hydride-based materials: development and optimisation

J.-C. Crivello¹ · B. Dam² · R. V. Denys³ · M. Dornheim⁵ · D. M. Grant⁶ ·
J. Huot⁷ · T. R. Jensen⁸ · P. de Jongh⁹ · M. Latroche¹ · C. Milanese¹⁰ ·
D. Milčius¹¹ · G. S. Walker⁶ · C. J. Webb¹²  · C. Zlotea¹ · V. A. Yartys^{3,4}

Received: 29 September 2015 / Accepted: 3 January 2016 / Published online: 27 January 2016
© Springer-Verlag Berlin Heidelberg 2016

Abstract Magnesium hydride has been studied extensively for applications as a hydrogen storage material owing to the favourable cost and high gravimetric and volumetric hydrogen densities. However, its high enthalpy of decomposition necessitates high working temperatures for hydrogen desorption while the slow rates for some processes such as hydrogen diffusion through the bulk create challenges for large-scale implementation. The present paper reviews fundamentals of the Mg–H system and looks at the recent advances in the optimisation of magnesium hydride as a hydrogen storage material through the use of catalytic additives, incorporation of defects and an understanding of the rate-limiting processes during absorption and desorption.

1 Introduction

Magnesium hydride (MgH₂) continues to be investigated as a potential hydrogen storage material due to the moderately high gravimetric and volumetric hydrogen density of $\rho_m = 7.6$ wt% H and $\rho_v = 110$ g H/l. In addition, this light metal is cheap and virtually limitless, i.e. occurs to an extent of 0.13 wt% in sea water and 2.76 wt% in the earth crust.

However, there are practical impediments to large-scale implementation of MgH₂-based hydrogen storage systems as the Mg–H system has unfavourable thermodynamics and slow kinetics for H₂ uptake and release. The thermodynamics dictates that relatively high temperatures must be

✉ C. J. Webb
j.webb@griffith.edu.au

✉ V. A. Yartys
volodymyr.yartys@ife.no; volodymyr.yartys@gmail.com

J.-C. Crivello
crivello@icmpe.cnrs.fr

B. Dam
B.Dam@tudelft.nl

R. V. Denys
roman.v.denys@gmail.com

M. Dornheim
martin.dornheim@hzg.de

D. M. Grant
David.Grant@nottingham.ac.uk

J. Huot
jacques.huot@uqtr.ca

T. R. Jensen
trj@chem.au.dk

P. de Jongh
P.E.deJongh@uu.nl

M. Latroche
latroche@icmpe.cnrs.fr

C. Milanese
milanese@unipv.it

D. Milčius
milcius@mail.lei.lt

G. S. Walker
Gavin.Walker@nottingham.ac.uk

C. Zlotea
claudia.zlotea@icmpe.cnrs.fr

¹ Université Paris Est, ICMPE (UMR 7182), CNRS, UPEC, 2 rue Henri Dunant, 94320 Thiais, France

² Delft University of Technology, Chemical Engineering, Delft, The Netherlands

³ Institute for Energy Technology, Kjeller, Norway

applied to desorb H_2 from pure MgH_2 , i.e. $T(1 \text{ bar}) = 283 \text{ }^\circ\text{C}$ calculated from the enthalpy and entropy change for bulk MgH_2 , $\Delta H_{\text{dec}} = 74.06 \pm 0.42 \text{ kJ/mol}$ and $\Delta S = 133.4 \pm 0.7 \text{ J/(mol K)}$ [1, 2].

Despite this, substantial progress in producing a practicable hydrogen storage material has been made, and the recent progress made in the past 5 years, especially in the framework of the International Energy Agency Task 32 Hydrogen-based Energy Storage, is reviewed in this paper.

Progress has, for instance, been made through nanostructuring [3, 4] and modifying with small amounts of catalytic additives. Nanoconfinement of MgH_2 clearly improves the kinetics of hydrogen release and uptake [5–7]. Nanostructuring by mechanochemical synthesis [8] introduces defects into the material which can enhance the kinetic rates, particularly for diffusion of hydrogen. Additives including transition metals, oxides and halides as well as carbons and others have also been found to significantly improve the reaction kinetics [9, 10]. Attempts to modify the thermodynamic properties of MgH_2 [11] have not been as successful. However, lower enthalpies have been reported for very small particle size ($<5 \text{ nm}$) [12] and nanoconfined structures in the form of thin films and encapsulated into porous carbons [13].

Magnesium forms a stoichiometric dihydride MgH_2 which crystallises in two polymorphic forms. Stable at ambient conditions, α - MgH_2 has a tetragonal TiO_2 rutile-type structure. This hydride, at high applied pressures exceeding 0.39 GPa (3.9 kbar) [14], transforms into a metastable, at normal conditions, γ - MgH_2 modification which crystallises with an orthorhombic α - PbO_2 -type structure. Further investigations using XRD reveal that different ball milling times led to the formation of the metastable orthorhombic γ - MgH_2 along with tetragonal α -

MgH_2 . The γ -polymorph can also be obtained by mechanochemical treatment of magnesium hydride [15]. A β - MgH_2 cubic modified CaF_2 structure has been also reported, observed experimentally using in situ synchrotron diffraction, which is stable at very high pressure [14].

During hydrogenation, the hexagonal close-packed (HCP) lattice of magnesium expands by approximately 30 % (31.4 for α - MgH_2 and 29.1 % for γ - MgH_2) (Table 1). The hydrogenation leads to a transformation of the HCP metal sublattice into the deformed body-centred cubic sublattice. Because of the deformation, this sublattice becomes tetragonal for α - MgH_2 and orthorhombic for γ - MgH_2 .

Even though the transformation α - γ is associated with a volume contraction by 1.3 %, the major features of the structures of the dihydrides remain similar for both hydrides.

If MgH_2 structures are considered as insertion-type compounds of hydrogen into the metal sublattice, one may conclude that hydrogen atoms in both cases have a coordination number of 3 being located in the centres of the Mg_3 triangles. From this perspective, MgH_2 does not resemble the features of the crystal structures of the transition metal hydrides where H atoms fill octahedral interstices [for atoms with atomic radii smaller than V (1.37 \AA)] or tetrahedral sites for larger size atoms ($r > 1.37 \text{ \AA}$). Thus, Mg behaves similar to aluminium; in both cases instead of filling the available interstices by H atoms, hydrogen becomes coordinated by a small number of the metal atoms (two in the structure of AlH_3 and three in MgH_2). This observation clearly reveals a significant degree of directionality and covalency in the bonding.

When it comes to the structure of the hydrogen sublattice, it appears that both MgH_2 polymorphs can be built from the same building blocks, namely the MgH_6 octahedra. These octahedra are more regular in case of α - MgH_2 , with just two types of Mg–H bonds, two axial (1.948 \AA) and four equatorial, slightly longer Mg–H bonds (1.952 \AA). In case of γ - MgH_2 , the MgH_6 octahedra appear to be more deformed and contain several Mg–H bonds spanning an interval 1.915 – 2.004 \AA . Because of a volume contraction on the transition α - MgH_2 and γ - MgH_2 , the shortest bond Mg–H is larger for α - MgH_2 (1.948 \AA) as compared to γ - MgH_2 (1.915 \AA) (see Table 2).

In the structure of α - MgH_2 , MgH_6 octahedra form infinite chains by sharing their edges (see Fig. 1). The neighbouring chains are connected between each other by sharing the vertices.

In the structure of γ - MgH_2 , the building principle of sharing the edges and vertices between the neighbouring octahedra, which is the case for α - MgH_2 , remains unchanged. However, instead of infinite MgH_6 chains, the simplest building blocks become pairs of MgH_6 octahedra connected by edges into a chain which are then linked together by the vertices forming a spacial framework.

⁴ Norwegian University of Science and Technology, Trondheim, Norway

⁵ Helmholtz-Zentrum Geesthacht, Zentrum für Material- und Küstenforschung GmbH, Geesthacht, Germany

⁶ Nottingham University, Nottingham, UK

⁷ Hydrogen Research Institute, Université du Québec à Trois-Rivières, Boulevard des Forges, Trois-Rivières, QC 3351, Canada

⁸ Interdisciplinary Nanoscience Center (iNANO) and Department of Chemistry, Aarhus University, Langelandsgade 140, 8000 Aarhus, Denmark

⁹ Debye Institute for Nanomaterials Science, Utrecht University, Utrecht, The Netherlands

¹⁰ Pavia Hydrogen Lab, C.S.G.I. and Chemistry Department, Pavia University, Pavia, Italy

¹¹ Lithuanian Energy Institute, Kaunas, Lithuania

¹² Queensland Micro- and Nanotechnology Centre, Griffith University, Brisbane, Australia

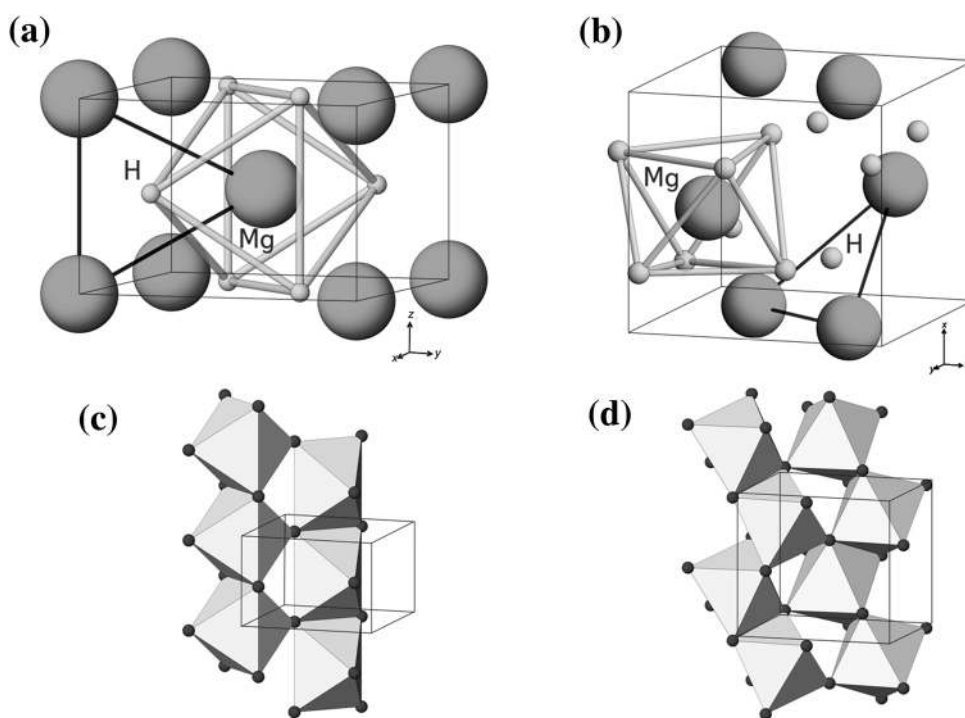
Table 1 Transformations in the metal sublattice during a transition Mg–MgH₂

Hydride	H/Mg	Metal structure	v_m (Å ³)	Hydride structure	References	v_h (Å ³)	$\frac{v_h - v_m}{v_m}$ (%)
α -MgH ₂	2	HCP	23.2	TiO ₂	[16]	30.53	31.4
γ -MgH ₂	2	HCP	23.2	α -PbO ₂	[17]	30.01	29.1

Table 2 Crystal structure data for α -MgH₂, β -MgH₂ and γ -MgH₂

Type of hydride	Space group of symmetry and type of structure	Unit cell parameters (Å)	Atomic coordinates	Shortest distances (Å)		Size of interstice r_{int} (Å)	References
				$D_{\text{Mg-H}}$	$D_{\text{H-H}}$		
α -MgH ₂	$P4_2/mnm$ TiO ₂	$a = 4.5025$ $c = 3.0123$ $V = 61.07 \text{ Å}^3$	2 Mg in 2a: 0; 0; 0 4 H in 4f: 0.306; x ; 0	1.948	2.471	$\Delta: 0.35$	[16]
β -MgH ₂	$Pa \bar{3}$ Deformed CaF ₂	$a = 4.6655$ $V = 101.55 \text{ Å}^3$	4 Mg in 4c: 0;0;0 8 H in 8c: 0.3429; x ; x	1.906	2.489	$\Delta: 0.37$	[17]
γ -MgH ₂	$Pbcn$ α -PbO ₂	$a = 4.5051$ $b = 5.4197$ $c = 4.9168$ $V = 120.06 \text{ Å}^3$	4 Mg in 4a: 0; 0.3313; $\frac{1}{4}$ 8 H in 8d: 0.273; 0.109; 0.079	1.915	2.489	$\Delta: 0.34$	[17]

Fig. 1 Crystal structures of α -MgH₂ (a); structure type TiO₂, space group $P4_2/mnm$; $a = 4.5025$; $c = 3.0123 \text{ Å}$; $d_{\text{Mg-H}} = 1.95$; $d_{\text{H-H}} = 2.47 \text{ Å}$ and γ -MgH₂ (b); structure type PbO₂, space group $Pbcn$; $a = 4.5051$; $b = 5.4197$; $c = 4.9168 \text{ Å}$; $d_{\text{Mg-H}} = 1.92$ – 2.00 ; $d_{\text{H-H}} = 2.49 \text{ Å}$. For both structures, a coordination of H atoms by 3 Mg atoms is shown. The hydrogen sublattice MgH₆ octahedra connect by edges in one direction forming a straight chain in α -MgH₂ (c); such a chain has a zigzag form (and runs along a screw twofold axis) in γ -MgH₂ (d). In both structures, the neighbouring chains are connected by sharing the vertices of the MgH₆ octahedra



2 Theoretical studies of MgH₂ and phase diagrams Mg–H (D, T)

The electronic structure of MgH₂ has been widely investigated by first principles approaches, such as the density functional theory (DFT). Because the α -MgH₂ and γ -MgH₂ structures are quite similar, with H atom located in the

centre of a triangle surrounded by 3 Mg, with Mg–H distances of about 2 Å, leading to very comparable electronic band structures [18]. The valence band width is about 7 eV, corresponding to the interaction of Mg 2*p*–3*s* states with the 1 *s* state of the two hydrogens. Since the equilibrium cell volume of the high-pressure γ -phase is slightly lower ($\sim 2 \%$) than the α -one, the orbitals are slightly more

localised for γ -MgH₂ (valence band width reduced by $\sim 5\%$). A charge transfer occurs from Mg to H. Bader charge analysis for both MgH₂ phases shows that Mg and H bear a charge of about $+1.62e$ and $-0.81e$, respectively.

The Mulliken effective charge analysis gives a more important transfer ($+1.87e$, $-0.93e$), and the bond overlap population (BOP) shows a small overlap [19]. Thus, unlike pure ionic hydrides like LiH, the Mg–H bonding interaction in MgH₂ is mainly ionic, but exhibits some covalent character. Figure 2 shows the electron localisation function (ELF) image of α -MgH₂ and illustrates that the covalent bond character between Mg and H is not dominating. It is, however, difficult to estimate the chemical bonding contribution depending on the methods and approximations: a rough estimation may lead to about 80 % ionic type. As a consequence, the cohesive energy is less important than for ionic hydrides like LiH, but still important in comparison with other metallic hydrides, such as LaNi₅H₆ with much weaker bonding. Adding another element, like a transition metal alloyed with MgH₂, may help to destabilise MgH₂ for practical use. Regarding the Fermi-level property, whatever the polymorphic structure is, the hydride remains of insulator type with a band gap of about 3–5 eV depending of the choice of the exchange–correlation functions [18].

In line with previous studies of the effect of pressure-induced polymorphic structural transition in MgH₂ [18], a study on the thermodynamics property has been recently led by Moser et al. [20]. Using the quasi-harmonic model, the free energy, bulk modulus and volumetric thermal expansion coefficient of the polymorphic hydrides have been calculated. Moreover, from both phonon calculations and experiments, the lattice parameters of MgH₂ and MgD₂ unit cell have been expressed as a function of temperature. This work has permitted the prediction of the structural

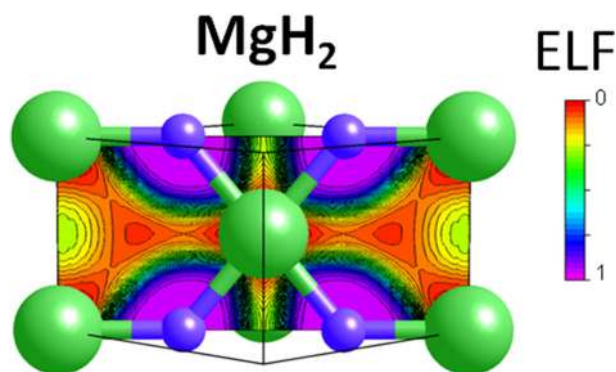


Fig. 2 Electron localisation function (ELF) image of the plane containing Mg and H atoms in α -MgH₂ ($P4_2/mnm$). Warm colour (red) areas indicate non-localised electrons (probability of presence close to 0), whereas cold colours (blue) represent strong localisation (probability of presence close to 1)

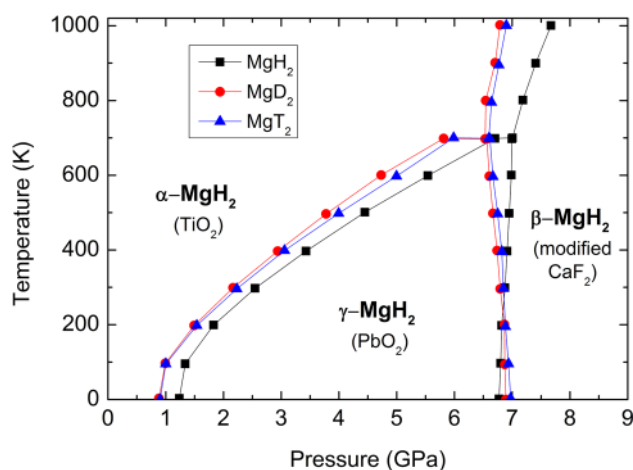


Fig. 3 Pressure–temperature (P – T) phase diagrams for the three polymorphs of magnesium dihydride studied for MgH₂, MgD₂ and MgT₂

transitions of MgH₂ under pressure with high accuracy and in agreement with neutron measurements. The Gibbs free energy as a function of the volume and temperature is also given and has allowed the computation of the (T , P) phase diagrams of MgH₂ as well as the isotopes MgD₂ and MgT₂ (Fig. 3). The temperatures of dissociation at different H₂ pressures are provided as well.

3 Properties of unmodified MgH₂

3.1 Thermodynamic properties of the Mg–H system

As for the other conventional hydrides, the equilibrium pressure of the $\alpha \leftrightarrow \beta$ transition is given by the Van't Hoff equation.

$$\ln P = \frac{\Delta H}{RT} - \frac{\Delta S}{R} \quad (1)$$

where ΔH and ΔS are, respectively, the formation enthalpy and entropy, P is the equilibrium pressure, T is the temperature and R is the gas constant. Magnesium hydride is considered to be a stable hydride, with a heat of formation of $-74.5 \text{ kJ}/(\text{mol H}_2)/\text{K}$ and entropy variation of $-0.135 \text{ kJ}/(\text{mol H}_2)$. Figure 4 shows the variation of plateau pressure as a function of temperature for magnesium hydride.

From Fig. 4, one can see that to desorb hydrogen under one bar of pressure, magnesium hydride has to be heated to at least 550 K. Similarly, magnesium could not absorb hydrogen below a pressure of 10 bar if the temperature is higher than about 640 K. It is thus clear that magnesium hydride could only operate at high temperature. The challenge is thus to reduce the temperature of operation while keeping as much as possible the high hydrogen storage

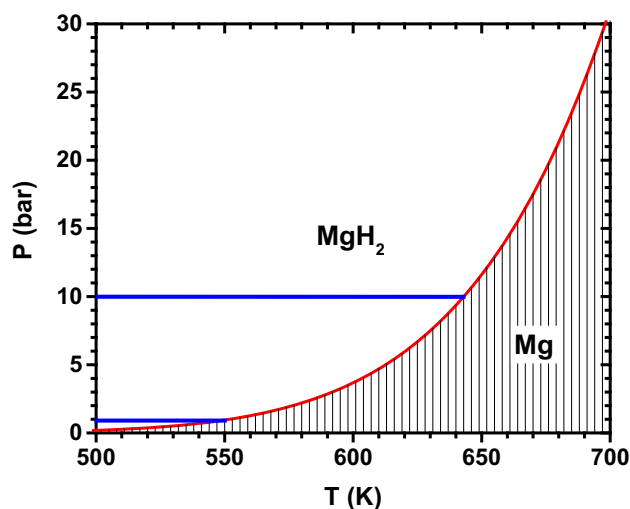


Fig. 4 Temperature dependence of the dissociation pressure of MgH_2

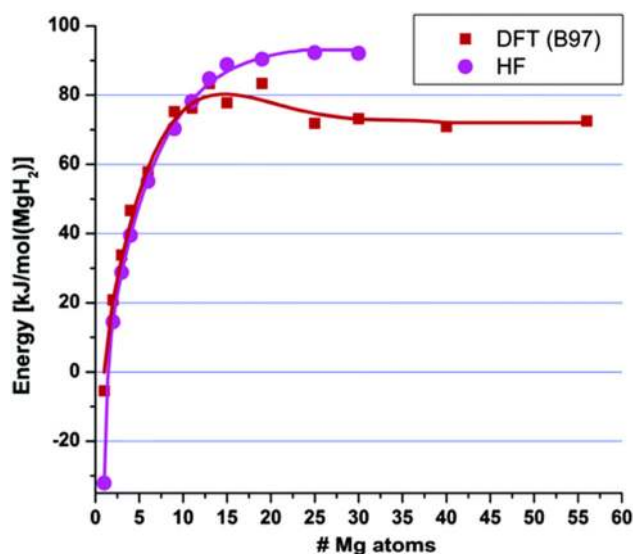


Fig. 5 Calculated desorption energies for MgH_2 clusters with both the Hartree–Fock (HF) and density functional theory (DFT) methods. The energies are normalised per mole of H_2 released. Reprinted with permission from [21]

capacity. One obvious solution is to alloy magnesium with another element (usually a transition metal). The classic example is Mg_2Ni where the heat of formation of the ternary hydride is reduced to $-64.5 \text{ kJ}/(\text{mol H}_2)$. Unfortunately, the capacity is also severely reduced to 3.6 wt%. Alloying with other elements has been studied but, as pointed out by Dornheim et al. [11] the chances of finding a new Mg-based intermetallic phase that forms a multicomponent hydride are small.

One possible way to change the thermodynamics of magnesium without changing the hydrogen capacity would be reducing the particle size as was demonstrated by Wagemans et al. [21]. Figure 5 shows the change of

desorption energy as a function of cluster size. It shows that reduction in energy is significant only for clusters smaller than 10 Mg atoms (about 0.9 nm). Calculations based on alternative approaches such as reactive force field [22], Wulff constructions [23] and surface energy differences [24] confirmed an expected lowering of the enthalpy of formation of MgH_2 for small particles.

Reduction in hydrogenation/dehydrogenation energy with crystallite size was measured experimentally by Paskevicius et al. [1] and by Zhao-Karger et al. [25], but the final outcome was smaller than the theoretical prediction and was counteracted by a decrease in entropy.

More recent theoretical investigations indicated that for MgH_2 , desorption energy actually increases with cluster size. Using a quantum Monte Carlo simulation, Wu et al. [26] found that clusters $(\text{MgH}_2)_n$ are more stable than the bulk for $n < 40$. More recently, Buckley et al. [27] used density functional theory (DFT) to estimate the desorption temperature under 1 bar of hydrogen. Their results also indicated that, even for clusters with $n = 64$, the desorption temperature is higher than for the bulk MgH_2 .

A very interesting new field of study is destabilised systems [28, 29]. In the Mg–Al system, it has been shown that, under hydrogen, the alloy $\text{Mg}_{17}\text{Al}_{12}$ presents reversible disproportionation reactions with the formation of MgH_2 at each step [30–33]. A destabilising effect has also been achieved by forming metastable Mg–Nb bcc alloy [34, 35] or with multilayers Mg–Ti [36, 37] or Mg–Al–Ti composites [38], but all of these systems suffer from a decrease in hydrogen capacity.

Recently, it has been shown that the formation of magnesium solid solution alloys with alloying elements such as In, Al, Ga and Zn could be an effective way to destabilise magnesium hydride [39]. For example, the desorption isotherm plateau at 1 bar is 20 K lower for a solid solution $\text{Mg}_{0.9}\text{In}_{0.1}$ compared to pure magnesium. Unfortunately, the hydrogen storage capacity also decreased to just less than 4 wt% H.

Destabilisation of magnesium hydride without important reduction in capacity is an important challenge. Many original avenues have been tried and showed promising results, but their main drawback is the important reduction in hydrogen capacity. Nevertheless, more research is needed especially in the fundamental aspect of this challenge.

3.2 Mechanisms of absorption and desorption

The reaction of Mg with hydrogen involves a number of different steps, such as physisorption, dissociation and chemisorption, the diffusion of hydrogen into subsurface sites and bulk lattice sites and finally the nucleation and growth of the hydride phase. During desorption, Mg itself has to be nucleated and hydrogen atoms have to diffuse to

the subsurface and surface and recombine there to hydrogen molecules, which have to be physically desorbed back into the gas phase. The overall hydrogen sorption kinetics is determined by the slowest step in this reaction chain [40]. While the diffusion constant of hydrogen in Mg has been found to be of the order of 10^{-13} m²/s at 300 K, H-diffusion in MgH₂ is found to be at least three orders of magnitude lower [41]. Hence, it is expected that during hydrogenation after the initial formation of a hydride layer around the Mg particles, the hydrogenation should slow down significantly. Indeed by measuring the hydrogen uptake and release of a variety of different samples with very small additive contents up to high additive contents and after applying very short ball milling time up to extended ball milling treatments, Barkhordarian et al. [42] could deduce the rate-limiting steps for both absorption and desorption. In case of absorption, they obtained the best fit to their data by applying a three-dimensional diffusion-controlled contracting volume model [43]:

$$1 - \left(\frac{2\alpha}{3}\right) - (1 - \alpha)^{\frac{2}{3}} = kt \quad (2)$$

with α being the transformed fraction and k the reaction constant. This equation should fit best those experimental data where diffusion through the transformed phase is the rate-limiting step as we would also expect from the H-diffusion through a Mg–Hydride layer.

In contrast to absorption, during H₂ desorption from samples with low catalyst/additive contents and very short milling times, Barkhordarian et al. [42] obtained the best fit by applying the surface reaction limited model:

$$\alpha = kt \quad (3)$$

hinting at the diffusion from subsurface to surface and the recombination of hydrogen atoms as the main rate-limiting steps in this process.

For pure α -MgH₂, a model of hydrogen evolution from the stoichiometric dihydride during its decomposition was proposed and successfully described the data of the thermal desorption spectroscopy study [44]. The model includes two steps: (1) formation of the nuclei of the metal phase, followed by (2) hydrogen evolution through the surface of the formed metallic islets. The latter stage is a limiting step of the overall process and determines the hydrogen desorption rate. For the partially hydrogenated magnesium, the first stage was absent, supporting the proposed mechanism of the desorption process.

3.3 Properties of powders: compaction and cycling

To evaluate the sorption behaviour of Mg and some Mg-based materials under compaction and cycling, powders of different compositions were milled in hydrogen gas and

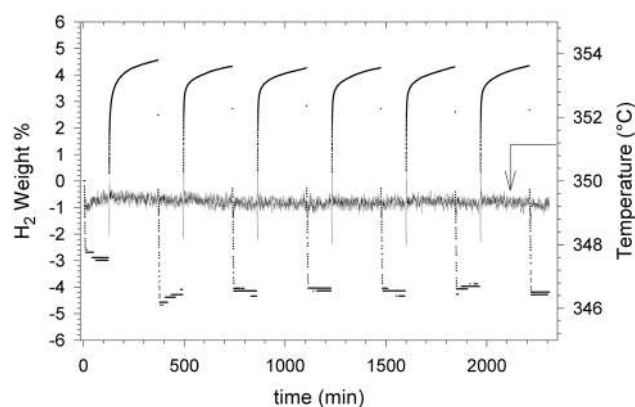


Fig. 6 Second discharge run and subsequently six charging/discharging cycles for a pure Mg pellet (kinetic and temperature profiles)

then were compacted at different pressures to obtain pellets. The pellets were cycled at 350 °C and 40 bar H₂/0.9 bar H₂ for 4 h hydrogenation/2 h dehydrogenation, respectively.

The sorption behaviour of a Mg powder (45–250 μ m) sample compacted at 140 MPa during is shown in Fig. 6. It is evident that the reversible H capacity is 4.3 wt% H and the cycling stability is high, with no visible decline in H storage performance. The H desorption–absorption process is completely reversible. After 40 cycles, the gravimetric capacity decreases by a factor of 1.5 and the absorption/desorption rates decrease by 1.5/2, respectively. By increasing the compaction pressure (the apparent density increases from 1.3 to 1.5 g/cm³), the absorption rate decreases by about 20 % and the desorption rate by 7 %.

When 15 wt% of Ni powder (45–150 μ m) was added to Mg, the reversible H storage capacity increased to 6 wt% of H in the conditions described above. This is a noticeably better performance than for the pure Mg sample. Increase in the compaction pressure to 420 MPa (the apparent density increased to 1.7 g/cm³) did not affect the amount of the exchanged hydrogen; however, the rates of H absorption–desorption became a little slower, with 4–5 wt% H₂ absorbed/desorbed.

The best results were demonstrated for a sample prepared with the same Mg:Ni ratio (85/15 wt%) after adding 5 wt% C/graphite (50 μ m) and 1.5 wt% TiO₂. The pellet reversibly exchanged 6.7 wt% H, with a 6 wt% H charge/discharge rate in 1.7/3.7 min. After 120 cycles, the gravimetric H capacity was unchanged. Very good sorption profiles were obtained for a ternary Mg–Nb₂O₅–graphitic C mixture (molar ratio % = 97.5:0.5:2.0), with a sorption capacity of 6.8 wt% H and a 6 wt% H absorption/desorption rate of 1.1 min/3.7 min (Fig. 7).

After the completed charge/discharge experiments, the cycled pellet samples remained compact in their central parts, with only some small pieces broken at the top. The

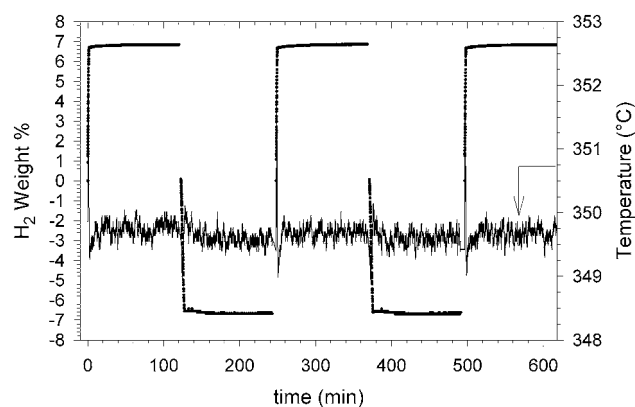


Fig. 7 Eighth–tenth charge/discharge cycles for a Mg–C–Nb₂O₅ pellet (kinetic and temperature profiles)

average variation in length of 30–40 % was independent of the number of the performed absorption–desorption cycles. The variation in diameter was 32 % for all pellets.

When performance of the pellets is compared with those of the powders with identical composition, it can be concluded that:

- the pellets store 0.2–0.3 wt% more hydrogen than the powders;
- considering the absorption kinetics, Mg–Ni-based pellets show better performance thanks to the presence of Mg₂Ni. The higher density results in a detrimental effect on the H₂ gas diffusion in Mg, while the enhancing effect of the Ni-containing phases has an opposite influence;
- Mg–Ni binary pellets show slower desorption kinetics than the powders, while for the ternary and quaternary systems containing C, the opposite behaviour is observed. This can be explained by considering two factors: the microscopic sorption mechanism of the dehydrogenation (refer above) and the variation in thermal conductivity. Concerning the first point, for the Mg–Ni samples, the rate-limiting step is hydrogen diffusion from the bulk to the surface. A higher compaction degree creates obstacles for the motion of hydrogen atoms between the layers of the active phases. When a carbon additive is present, the highest aggregation of the active species becomes an advantage. The thermal conductivity average values increase from 0.18 W/(m K) for the binary powder mixture to 0.22 W/(m K) when C is added, and, eventually, to 0.36 W/(m K) when the mixtures are compacted. This variation leads to a better heat transfer, thus enhancing the absorption kinetics.
- Pellets show a better cycling behaviour than the corresponding powders. For the powders, the degradation could probably be attributed to the grains sintering during the thermal treatments.

4 Mechanical modification

4.1 Ball milling

Mechanochemical synthesis using ball milling of magnesium hydride with and without additives and alloying metals has been employed to produce defect-enhanced potential hydrogen storage materials [8]. The high-pressure, high-energy impacts of the balls and vial walls repeatedly compress, fracture and cold-weld the powder particles. This can significantly reduce both powder and grain (crystallite) size, break the oxide layer on magnesium powder and provide fresh surfaces, as well as dispersing additives through the composite materials. Reactive ball milling (RBM), ball milling under a hydrogen atmosphere, is a convenient way to produce many hydrides. The high mechanical pressures can, in general, induce high-pressure polymorphs of the powder, and in particular, the metastable gamma phase of MgH₂ is frequently observed after ball milling. Alloying can be readily achieved by milling. Some alloys, such as magnesium-iron alloys, have only been synthesised by ball milling. The milling process involves several parameters such as the type of ball mill, (planetary, shaker, attritor), the ball-to-powder ratio, milling speed, time, temperature, milling atmosphere and pressure [45] as well as volume ratio [46]. The large number of parameters, the range of values for each parameter and the fact that they are not always adequately reported makes it difficult to compare results from materials synthesised in different laboratories. Ball milling of magnesium metal in hydrogen gas results in the in situ formation of a mixture of α - and γ -MgH₂ and decreases the temperature of hydrogen desorption as compared to conventional MgH₂ [47].

4.2 Severe plastic deformation

Severe plastic deformation (SPD) is a general term used to describe a group of techniques that produce large strains in the material which in turn result in a high defect density and nanocrystalline structure. The SPD techniques could replace and/or complement high-energy milling for the synthesis and preparation of metal hydrides. The advantages of SPD over the ball milling are that usually SPD can be easier to scale up to industrial level, the impurity level is lower, and it has fewer safety concerns [48]. The use of SPD techniques in the processing of metal hydrides is relatively new, and this field of research is rapidly developing. For the processing of magnesium-based alloys, the popular SPD techniques are: equal channel angular pressing (ECAP), high-pressure torsion (HPT) and cold rolling (CR). Here, we will focus on one of these: ECAP.

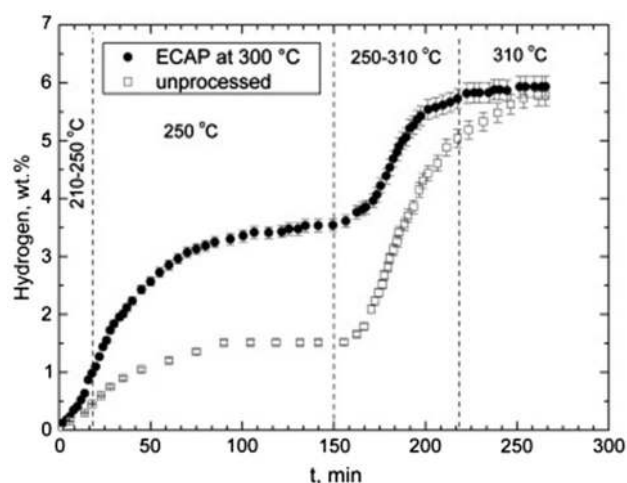


Fig. 8 Hydrogen desorption kinetics from the unprocessed and ECAP processed (300 °C) samples of ZK60 observed in the temperature range from 210 to 310 °C. Reprinted with permission from [50]

4.3 Equal channel angular pressing

The first use of ECAP on Mg-based alloys was performed by Skripnyuk et al. [48–51] who found that after ECAP followed by high-energy milling, the hysteresis in the pressure–composition isotherm completely disappeared and hydrogenation kinetics were improved. Since these early studies by Skripnyuk, a number of groups have investigated magnesium and magnesium-based alloys processed by ECAP or a combination of ECAP and another SPD technique. For example, a combination of ECAP and high-energy milling was used by Løcken et al. [52] on the ternary eutectic Mg–Mg₂Ni–MmMg₁₂ (72 wt% Mg–20 wt% Ni–8 wt% Mm, Mm = mischmetal), and by Révész et al. [53] on Mg–Ni. These studies found that kinetics are improved, but the impact on the thermodynamics was negligible.

In an early investigation on the effect of ECAP on the magnesium alloy ZK60 (composition: 5 wt% Zn; 0.8 wt% Zr; Mg balance), Skripnyuk et al. [50] showed that ECAP greatly improved the hydrogenation kinetics as shown in Fig. 8. This was confirmed by Krystian et al. [54] who found that ECAP increases the hydrogenation kinetics, but again, this was not accompanied by a change of the thermodynamics of hydride formation.

In a study on the combined effect of ECAP and CR on magnesium, Jorge Jr et al. [55] found that after ECAP the hydrogen capacity is very small but greatly increases when ECAP is followed by CR. They also showed that when magnesium has a (002) texture, its hydriding kinetics are enhanced.

ECAP and other SPD techniques represent a new and powerful way to modify the hydrogenation kinetics of

metal hydrides. However, the prospect of using these techniques to destabilise magnesium hydride is not so obvious. Nonetheless, SPD techniques should be investigated further for the development of new metal hydrides.

4.4 Rapid solidification

Rapid solidification (RS) allows the nanostructuring of the hydrogen storage materials which results in a dramatic positive effect on the H sorption behaviours. The microstructure and grain size of the materials produced by RS depend on the rotation speed of the wheel determining the cooling rate in the solidified alloy. For the Mg-rich alloys with rare earth metals (mischmetal) and nickel, the conditions of RS strongly influence the particle size of the formed particles, spanning a broad range of sizes, from 50 nm to 1 µm. The most detailed studies were performed for the La(Mm)NiMg alloys obtained by RS at different cooling rates, RS300, RS1000 and RS2000 (corresponding to surface velocity 3.1, 10.5 and 20.9 m/s) [56–58]. The hydrogenation properties of the alloys appear to be strongly related to the solidification rate/nanostructuring. In the RS2000 alloy, the smallest particle sizes were observed (using TEM), and this correlates with advantageous hydrogenation behaviours of the material. The highest hydrogenation rate was observed for materials which were solidified with the highest cooling rate [56, 57].

The effect of nanostructuring achieved by rapid solidification on the hydrogen storage performance can be illustrated by taking an example of the Mm-10Ni-2 Mm alloys (see Fig. 9).

The changes in particle size cause significant variations in the rates of hydrogen exchange in the materials.

Micrographs of Mg-20Ni-8 Mm produced with a surface velocity of the copper wheel of 3.1 m/s are presented in Fig. 10. Mg and Mg₂Ni particles elongated with a length from 250 to 1.5 µm in one direction are clearly visible on the TEM micrograph of the overall morphology of the RS alloy. The width of the particle is about 200 nm (see Fig. 10a). A highly magnified area with Mg and Mg₂Ni crystallites with an average size of 200–400 and 200–1000 nm, respectively, is shown in Fig. 10b. The highest surface velocity of the wheel gives an extremely high cooling rate of the materials leading to amorphisation [58].

In the Mg-rich alloys of La, containing LaMg₁₂ and La₂Mg₁₇ compounds, with increasing solidification rate the alloys were formed in the microcrystalline (RS300), nanocrystalline (RS1000) or amorphous state (RS2000). This directly influences the mechanism of H absorption and desorption with a reversibility of the formation of the initial intermetallics for the nanostructured hydrides or irreversible disproportionation to form Mg and LaH₂ on hydrogen desorption [59–61].

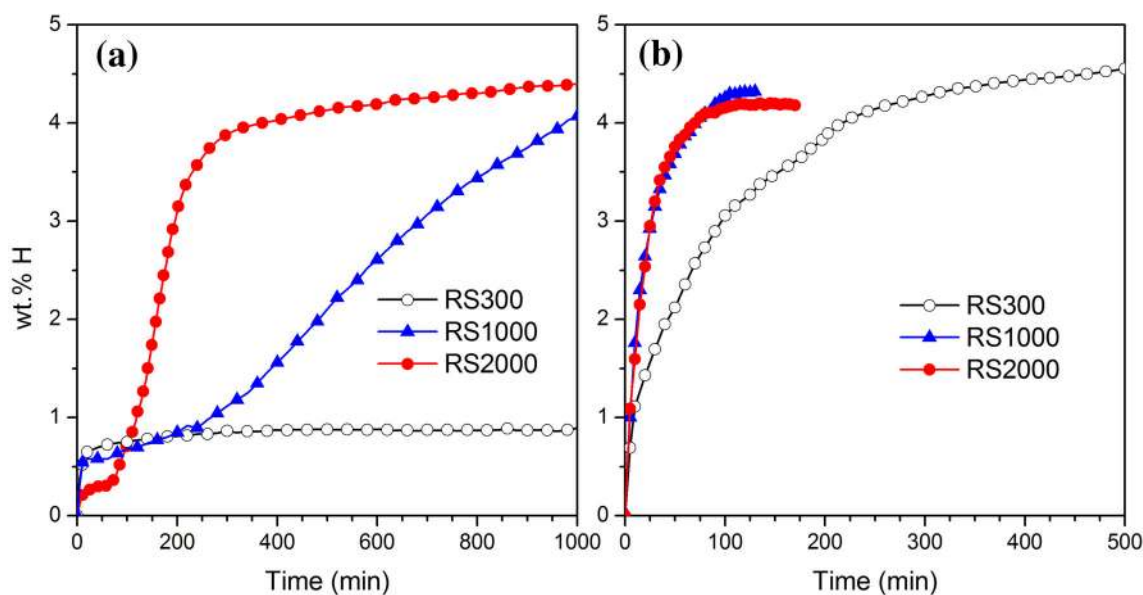


Fig. 9 Comparison of hydrogen absorption characteristics of the melt-spun Mg-20Ni-8 Mm alloy (solidified on a copper wheel at rotation speeds 300, 1000 and 2000 rpm) at 300 °C and 28 bar H₂:

a hydrogenation curves of the first cycle and **b** hydrogenation curves after five hydrogenation/dehydrogenation cycles

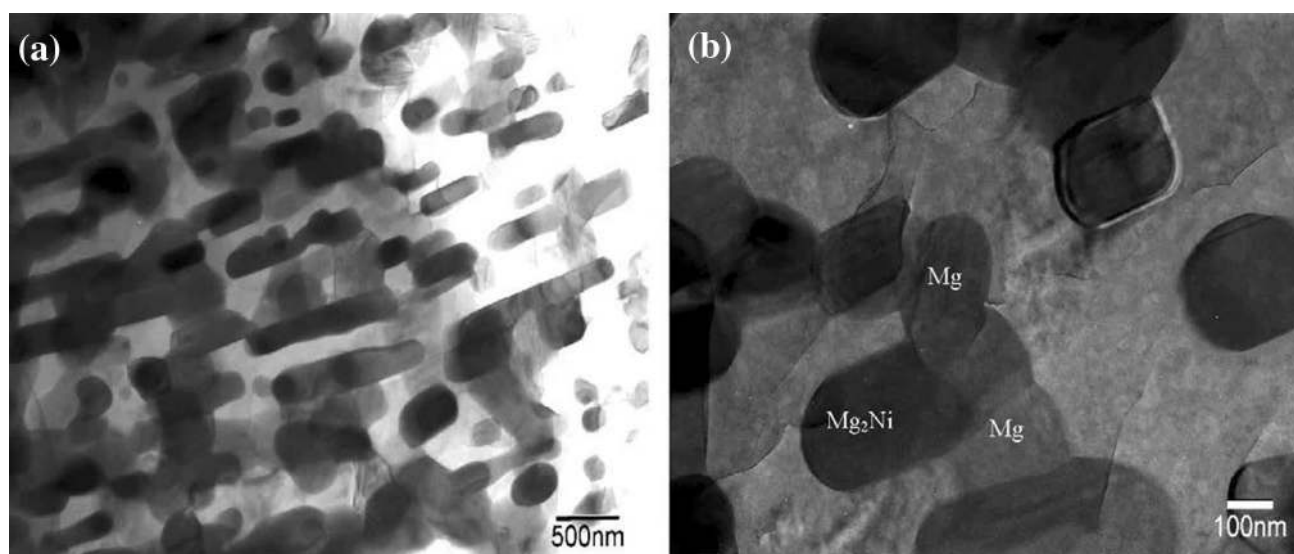


Fig. 10 TEM micrographs showing the microstructures of melt-spun Mg-20Ni-8 Mm produced with a surface velocity of the copper wheel of 3.1 m/s: **a** overall morphology and **b** high magnification image of Mg₂Ni and Mg particles

4.5 Nanoconfinement

To modify the sorption properties of magnesium or magnesium alloys, the use of particle confinement [62–65] has been proposed. By increasing the surface-to-bulk atomic ratio, changes in the thermodynamics are foreseen. However, handling nanoparticles of metals or hydrides is very challenging and this is commonly done using a porous scaffold to stabilise the particles and to prevent them from coalescence [66].

The first systematic study of the kinetics of hydrogen sorption as a function of particle size was conducted by Au et al. [67], using 6–20 nm MgH₂ particles in carbon aerogels. As shown in Fig. 11, the hydrogen release temperature showed a clear and systematic size dependence, and the onset of desorption was ~150–200 °C lower for the nanoparticles than for macrocrystalline MgH₂. This was corroborated by intrinsic hydrogen dynamics obtained by solid-state ¹H NMR. Cycling was fast (80 % of the capacity absorbed within 15 min at 300 °C and 18 bar H₂),

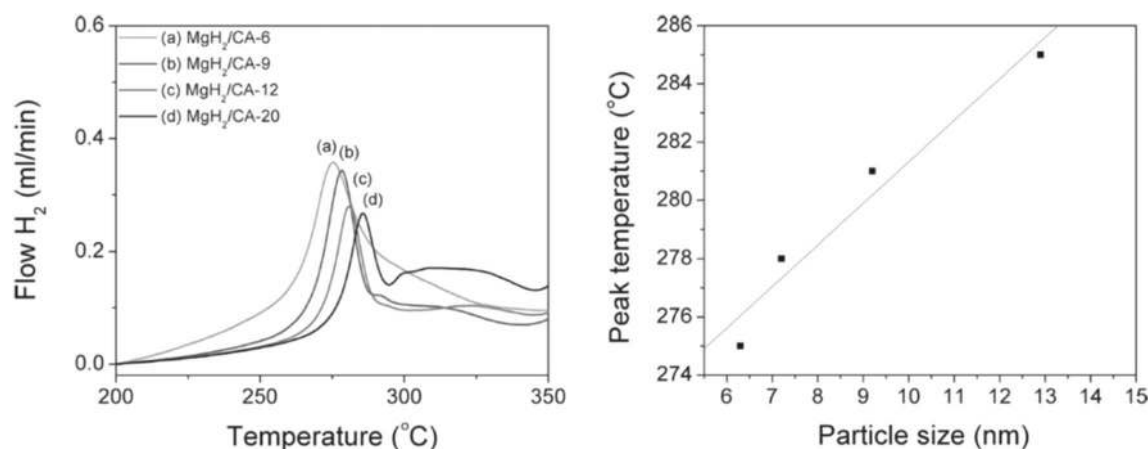


Fig. 11 *Left* Hydrogen release for carbon aerogel-supported MgH_2 particles with different sizes as indicated, scanning with 5 $^{\circ}C/min$ in Ar flow. *Right* relation between peak release temperature and particle size. Figure adapted from [67]

and there was no change in sorption properties upon cycling, showing that the growth of the particles is effectively prevented by the carbon support.

These results were extended to smaller particles by Zlotea et al. [68] using ordered microporous carbon and tuning the Mg amount from 15 to 50 wt%. Ultra-small particles with mean sizes of 1.3 and 3.0 nm have been obtained for 15 and 25 wt% Mg contents, respectively. The hydrogen desorption properties strongly depend on the nanoparticle size, as evidenced by different thermal analysis techniques. The onset temperature of hydrogen desorption for MgH_2 nanoparticles below 3 nm occurs at a temperature about 245 K lower than for microcrystalline material. Two distinct hydrogen desorption peaks are noticed for nanoparticles with mean sizes of 1.3 and 3.0 nm, as confirmed by TDS and HP-DSC. 1H NMR investigations suggest the presence of two MgH_2 populations with enhanced hydrogen mobility, as compared to the microcrystalline hydride. The short hydrogen diffusion path and the enhanced hydrogen mobility may explain the increased desorption kinetics of these ultra-small nanoparticles.

Intermetallic Mg_2Ni and its hydride Mg_2NiH_4 nanoparticles were prepared and stabilised into the mesopores of a template carbon [64, 69]. One approach was to first deposit well-defined Ni nanoparticles inside the pores, followed by vapour-phase deposition of Mg and hydrogenation. Alternatively, this was achieved by first forming Ni and MgH_2 particles inside the mesopores. Then by setting the temperature and the hydrogen pressure, the formation of either the intermetallic or the hydride was obtained. At low pressure (<0.5 MPa), the Mg_2Ni is formed by hydrogen release from MgH_2 , forming pure Mg able to react with Ni. Then, hydrogenation leads to Mg_2NiH_4 at pressures above 0.5 MPa. At high pressure

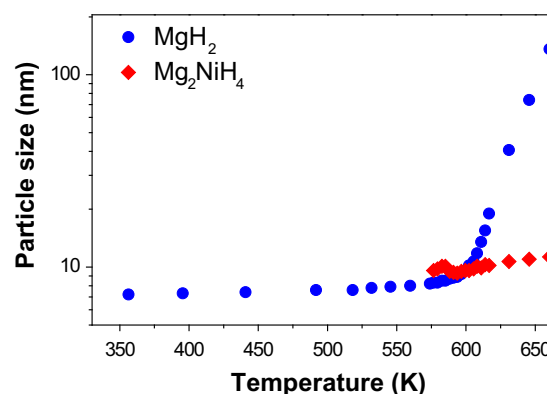


Fig. 12 Thermal variation of the average crystallite sizes of Mg_2NiH_4 and MgH_2 during heating with 2 K/min from 300 to 660 K under 2 MPa of H_2

(2 MPa), Mg_2NiH_4 is formed directly in a single step from the initial MgH_2 and Ni nanoparticles. The hydrogen sorption in nanosized Mg_2Ni is found to be reversible, and moreover, the formed hydride is able to desorb in a very short time at a low temperature (483 K).

The work of Zlotea et al. [64] showed that contrary to MgH_2 , the size of the nanoparticles of Mg_2NiH_4 is not affected by sorption cycling nor by high temperature. Indeed, Fig. 12 shows a constant average size for the Mg_2NiH_4 (11 ± 2 nm) in the temperature range 570–660 K, contrary to MgH_2 for which a sharp increase in the size up to 200 nm is observed between 570 and 660 K. This indicates that Mg has a larger mobility at high temperature leading to larger particles. When alloyed with Ni, its diffusivity is markedly reduced and both Mg_2Ni and Mg_2NiH_4 nanoparticles are stable upon prolonged exposure to high temperature and hydrogenation/dehydrogenation cycling.

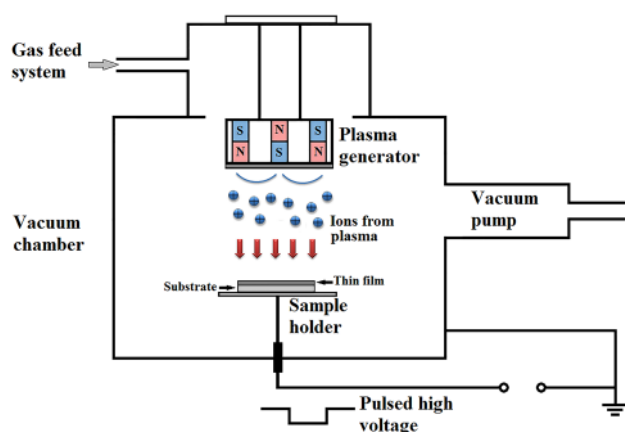


Fig. 13 Plasma-based hydrogenation approach

Nanoconfined Mg_2NiH_4 exhibits higher desorption kinetics by comparison with other $\text{Mg}_{1-x}\text{Ni}_x\text{H}_y$ nanocrystals supported on carbon; however, the thermodynamics properties are not altered by nanoconfinement.

4.6 Synthesis of MgH_2 using hydrogen plasma-based hydrogenation approach

Contrary to traditional methods for MgH_2 formation including top layer Pd catalyst deposition onto Mg and hydrogenation at high hydrogen pressures and temperatures [70] or formation of MgH_2 during extensive ball milling procedures, hydrogen could be introduced into Mg using plasma-based technologies. Using this approach, Mg in the form of thin films or powders is inserted in hydrogen plasma and sustains intensive bombardment of hydrogen ions (Fig. 13) which could lead to the formation of H-rich altered layers in near surface region or formation of MgH_2 in the depths of the material. Furthermore, even if surface contamination (in the form of oxides, hydroxides etc.) is present on the metal surface before hydrogenation, this could be removed during reduction reactions or by physical sputtering induced by energetic ions arriving from the plasma and lead to further extensive hydrogenation of Mg-based materials.

The described plasma-based approach was successfully used for the magnesium films and, also, in the case of hydrogen insertion into Al helping to avoid $\text{Al}(\text{OH})_3$ formation on the surface when applying the electrolytic charging procedure [71]. In spite of all potential benefits of the plasma hydrogenation procedure, the latest work on the hydrogenation of the Mg thin films demonstrated its limitations. This work revealed that the Mg oxide and hydroxide layer are formed and effectively block the formation of the hydride, even if its formation might be starting not at the surface but at the film–substrate interface and/or bulk of the film [72].

4.7 Thin films as model systems for thermodynamic and kinetic properties

The optical changes in thin Mg films on hydrogenation allow for a combinatorial analysis of the thermodynamics of the hydrogenation process as a function of composition. In the Mg–Ti–Ni system, the hydrogenation pressure, enthalpy and entropy of hydrogenation can be mapped [73]. While the enthalpy is remarkably low, the hydrogenation pressure remained at around 10 mbar, due to surprisingly low entropy. The complex, quasi-amorphous nature of these films precluded a clear explanation of this. This shows that an in-depth microstructural analysis is needed in conjunction with the hydrogenation results for a proper interpretation.

A much clearer picture arose for the Mg–Ti system. Here, it was found that beyond a critical Ti fraction of 15 %, a coherent mixture of MgH_2 and TiH_2 is formed [74]. While this coherent ordering could not be reproduced in bulk samples, the formation of small patches of TiH_2 in the MgH_2 matrix was verified by EXAFS [75]. While the effect of the Ti on the enthalpy of formation of MgH_2 is small, preliminary experiments on Ti-rich (75 %) samples show a much larger effect of the Ti on the hydrogenation pressure of Mg. This is explained by a much higher fraction of interfaces with respect to the volume of Mg in these samples [76]. At a Ti fraction of 75 %, a coherent structure was observed. Also, for this composition in bulk, a single FCC hydride phase was observed [77].

Thin films provide a means to analyse the effect of surface energy, strain and plastic deformation on the hydrogenation kinetics and thermodynamics in a controlled way. Nanosizing may result in a modification of all three terms, which makes it often difficult to estimate the contribution of these terms to the destabilisation which one aims for. Analysing pressure–composition isotherms, it should be stressed that the first two effects give a shift in both branches of the hydrogenation hysteresis, while plastic deformation results in widening of the hysteresis. Therefore, one cannot conclude much on the basis of a shift in the plateau pressure of only one of the branches.

Using a Ti/Mg/Ti/Pd multilayer thin film with a gradient Mg thickness, Mooij et al. [36] found that both the hydrogenation and dehydrogenation plateau pressure depend on the thickness. They deduced this to be the result of a change in the Mg/Ti interface energy on hydrogenation of around 0.35 J/m^2 . From similar experiments on Fe/Mg/Fe/Pd multilayers [78], a much higher interface energy was deduced, although the effect was partly obscured by the diffusion of Pd through Fe. Much larger effects of the thickness on the plateau pressure were found in Mg/Pd multilayers. At first, it was claimed that this was the result of stress [79] or destabilisation due to alloying [80]. Since

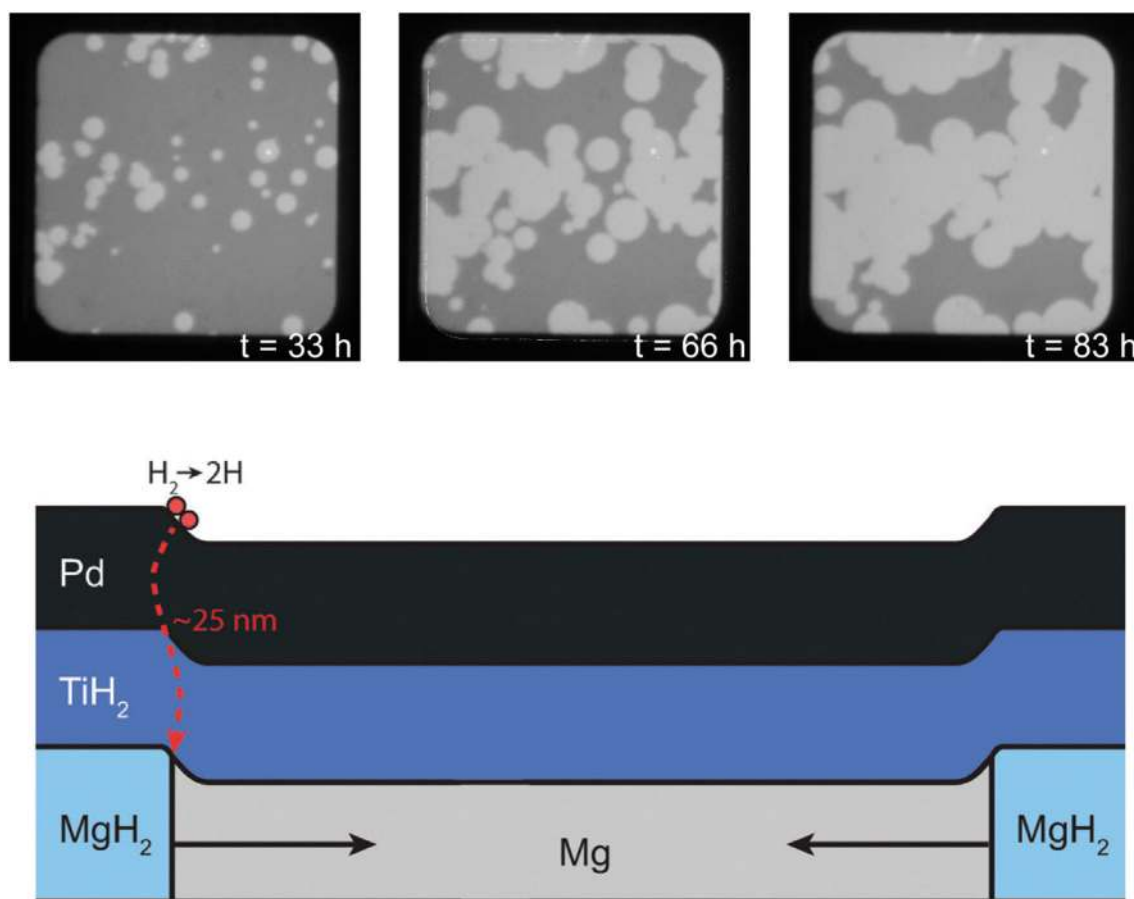


Fig. 14 *Top* Images of the 10×10 mm thin-film Ti/Mg/Ti/Pd multilayer samples in optical transmission after multiple hours of exposure to hydrogen ($p(\text{H}_2) = 70$ Pa, $T = 363$ K). The MgH_2 domains transmit more light and are brighter. Over time, the islands

grow bigger, while new nuclei are still being formed. *Bottom* schematic representation of the deformation taking place at the edges of the hydrogenated islands, due to the 30 % volume expansion of MgH_2 (figure based on [81])

this destabilisation effect was not found on dehydrogenation, it is now believed that in the case of interface alloying, plastic deformation plays a crucial role.

In the case of a multilayer Ti/Mg/Ti/Pd system where such interface alloying does not take place, plastic deformation still plays a role. Here, it mainly affects the kinetics of the hydrogenation [79]. Optical transmission images of the films taken at a pressure slightly below the hydrogenation plateau clearly show the nucleation and growth behaviour of Mg starting from preferential nucleation sites (Fig. 14). Optical analysis shows that this nucleation and growth behaviour also takes place at much higher driving forces. From an analysis of the relation between the step curvature and the expansion of the nucleating islands, the reduction in the kinetics of the phase transformation process due to the plastic deformation could be quantified [81]. The retardation of the kinetics of the phase transformation process is believed to be due to the deformation of the film stack that is needed to accommodate the 30 % volume expansion, which mainly takes place in the direction normal to the film. We speculate

that such a reduction in the kinetics also takes place in melt-infiltrated nanocrystals, which are bound to be strongly affected by plastic deformation.

4.8 Additives for catalytic enhancement

Addition of comparatively small amounts of another material to MgH_2 has been shown to be highly successful in improving the rates at which MgH_2 absorbs and desorbs hydrogen. Most additives do not absorb hydrogen themselves, and so they add mass to the composite sample with no corresponding uptake which reduces the overall gravimetric capacity of the sample. A large variety of different kinds of additives have been tested, including various types of carbon [82, 83], metal and non-metal elements, oxides, halides, intermetallics, hydrides [84] and others (carbides, nitrides and borides) [9]. When the added element has a large reaction enthalpy of hydrogenation like vanadium, the Mg-based composites prepared by reactive ball milling exhibit explosive, “combustion”-type hydrogenation when

the saturated hydride composites are formed in just seconds [85]. The most successful of these additives has been Nb_2O_5 , which was first used by Barkhordarian et al. [86]. Although other additives such as TiN and TiC have been shown to produce similar results [87], Nb_2O_5 is still held as a benchmark material as an additive to MgH_2 .

The improvement in hydrogen absorption and desorption is primarily in the rates of the metal-hydrogen reactions. With increased rates of reaction, both absorption and desorption can proceed at lower temperatures than the uncatalysed material. Although there have been individual reports of enhanced thermodynamics using additives TiH_2 , attributed to the 5–10 nm grain size [88] and LaH_3 , attributed to strain of MgH_2 when the adjacent LaH_3 phase released H_2 [89], the majority of investigations report no change in the enthalpy with catalytic additives [9].

Unfortunately, the use of magnesium hydride is hindered by several factors that mediate slow kinetics for hydrogen release and uptake. The surface oxide layer (MgO), which covers magnesium metal, is considered almost impermeable to hydrogen and decreases the kinetics significantly [90].

4.9 Niobium pentoxide additive

Niobium pentoxide, Nb_2O_5 , has proven to be one of the most effective additives mediating complete hydrogen release and uptake within 90 and 60 s, respectively, at 300 °C [91–95].

The literature provides many different explanations for the positive effects. (1) Niobium pentoxide may act as a dispersive agent during ball milling, which leads to a smaller average particle size of MgH_2 [92]. Particle size reduction of MgH_2 down to the nanometre scale, e.g. by nanoconfinement in nanoporous materials or an alkali-metal halide matrix, mediates enhanced reaction kinetics and improves thermodynamic properties [4, 5, 25]. (2) Niobium pentoxide can also act as an active reservoir that splits and transports the hydrogen molecule in or out of Mg/MgH_2 [96]. (3) The prolific properties have also been linked to the stability, i.e. Nb_2O_5 is not easily fully reduced to niobium metal [95], although niobium (4) is observed to be partially reduced during ball milling and upon hydrogenation and dehydrogenation of Mg/MgH_2 cycles at elevated temperatures. Upon decomposition, Nb_2O_5 may form ternary Mg – Nb oxides, which are suggested to facilitate hydrogen diffusion through the surrounding magnesium oxide surface layer [97–99]. The effect of Nb_2O_5 for hydrogen release and uptake in the Mg/MgH_2 system has been investigated using in situ SR-PXD [100, 101] of three MgH_2 – Nb_2O_5 (8 mol %) samples continuously ball-milled to different extents during up to eight full hydrogen release and uptake cycles [102]. The aim of this study was to explore the chemical reactions in the system Mg – MgH_2 – Nb_2O_5 with relative large amounts of additive and to develop further knowledge on the superior properties of niobium pentoxide as an additive. An example is provided in Fig. 15 [102].

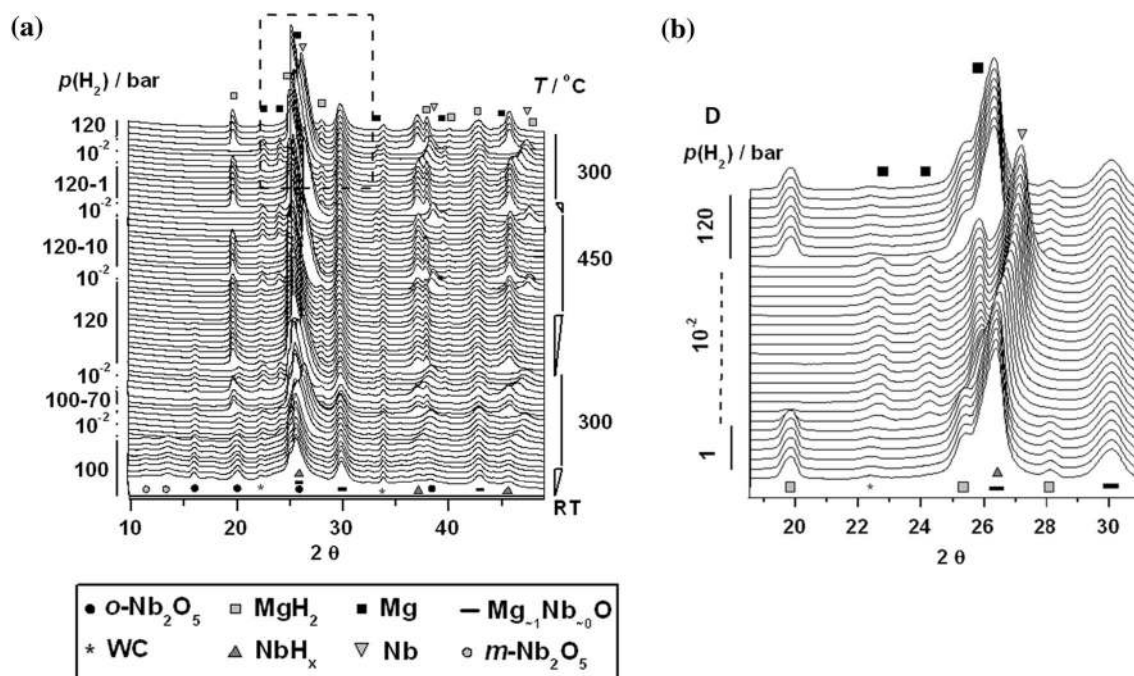
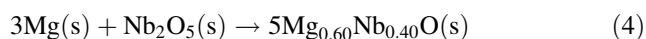


Fig. 15 **a** In situ SR-PXD data of MgH_2 – Nb_2O_5 (8 mol %) showing the hydrogen release and uptake from sample S3 heated stepwise from RT to 300 and 450 °C at variable hydrogen pressure are varied

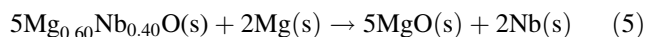
$p(\text{H}_2) = 10^{-2}$ or 120 bar. **b** Hydrogen release and uptake in sample S3 showing cycle 5, $T = 300$ °C after heating to 450 °C. Time propagates from bottom to top ($\lambda = 1.09801$ Å) [102]

4.9.1 Chemical reactions in the $\text{MgH}_2\text{--Nb}_2\text{O}_5$ system

Dynamic studies of hydrogen release and uptake using in situ SR-PXD experiments may allow the determination of intermediates with overlapping reflections, which may form at different rates and at different p , T conditions [102]. Rietveld refinement analyses suggest that a reaction between MgH_2 and Nb_2O_5 occurs during sample preparation (BM), which produces the ternary oxide $\text{Mg}_x\text{Nb}_{1-x}\text{O}$. Such a reaction may explain the fact that all published diffraction data only reveal the presence of one solid oxide. At elevated temperatures, a reaction between Mg and Nb_2O_5 occurs forming a ternary oxide. A composition of the ternary solid solution, $\text{Mg}_{0.60}\text{Nb}_{0.40}\text{O}$, is obtained when the reaction scheme is balanced assuming an oxidation state +2 for Nb (see Eq. 4), which may indicate an upper limit for the niobium content in the solid solution of 40 mol %.



More extreme mechanochemical conditions or cycling of the $\text{MgH}_2\text{--Nb}_2\text{O}_5$ composite with hydrogen release and uptake at $T > 300^\circ\text{C}$ may lead to formation of niobium or niobium hydride, i.e. niobium is extracted from the ternary solid solution by reduction of Nb(II) as illustrated in reaction scheme (Eq. 5). Finally, MgO (or $\text{Mg}_{\sim 1}\text{Nb}_{\sim 0}\text{O}$) and Nb will form [102].



The niobium-oxygen chemistry is diverse with a variety of different oxides with niobium present in oxidation states from five to two, but the PXD data measured in this study

suggest that niobium is present only in oxidation state five in the niobium pentoxides and two in the ternary solid solutions. However, a previous study proposed an average oxidation state of 2.5 for Nb realised by niobium with oxidations states +2 and +3 [98]. Previous studies reveal that annealing of $\text{MgH}_2\text{--Nb}_2\text{O}_5$ mixtures at 400°C leads to a decrease in the gravimetric hydrogen storage capacity of the system and also a reduction in desorption kinetics [95, 98]. Our investigation shows that this may be due to increasing amounts of Mg in the ternary oxide and eventually due to the formation of $\text{Mg}_{\sim 1}\text{Nb}_{\sim 0}\text{O}$. Formation and stabilisation of the ternary oxide appear to be important for the prolific kinetic effect of Nb_2O_5 as an additive in magnesium hydride [99]. Furthermore, diffusion of hydrogen through bulk niobium inclusions in MgO may be faster than diffusion in bulk MgO (see Fig. 16b).

Previous studies reveal sample activation and improved kinetics for hydrogen release and uptake in the $\text{MgH}_2\text{--Nb}_2\text{O}_5$ system upon cycling at $T = 300^\circ\text{C}$ [103]. The results presented here suggest that Nb_2O_5 reacts with Mg and forms a ternary solid solution $\text{Mg}_{0.60}\text{Nb}_{0.40}\text{O}$, which can be stabilised by relatively mild ball milling conditions and moderate working temperature, $T \leq 300^\circ\text{C}$. We anticipate that the reactions observed here at higher temperatures ($>300^\circ\text{C}$) may also occur at lower temperatures, e.g. at 300°C , but over a longer timescale during many hydrogen exchange cycles.

Rietveld refinements and the stoichiometry are plotted as a function of hydrogen release and uptake cycle number in Fig. 16a. The initial Mg content in the ternary solid solution is $\text{Mg}_{0.2}\text{Nb}_{0.8}\text{O}$, see Fig. 16a. The relative Mg

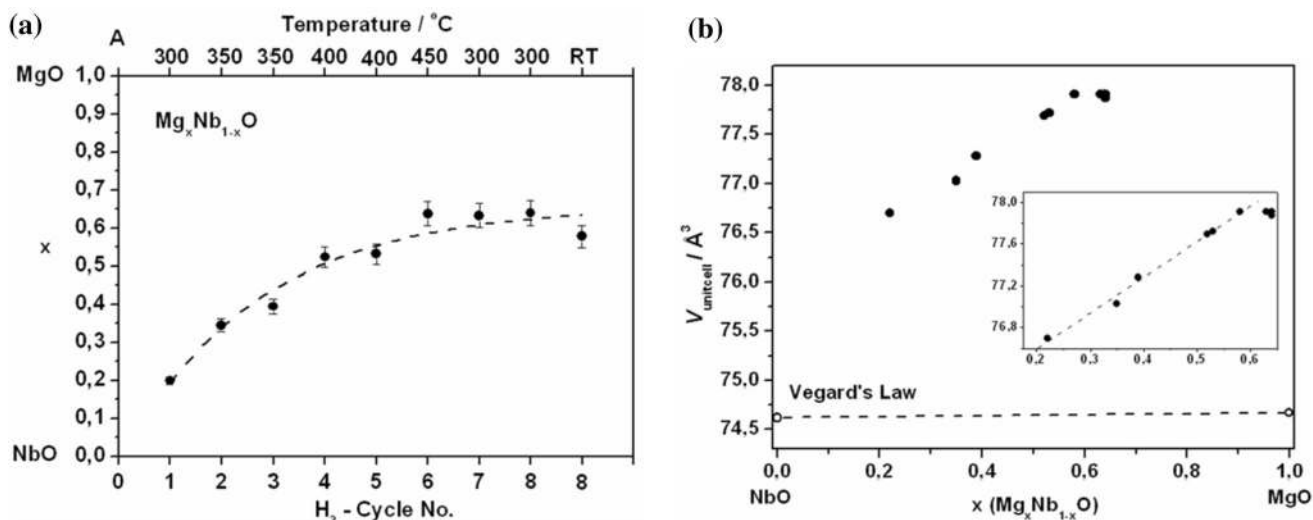


Fig. 16 **a** Composition of the solid solution $\text{Mg}_x\text{Nb}_{1-x}\text{O}$ obtained by Rietveld refinements (black circles) of selected SR-PXD diagrams (the dashed line is a guide to the eye). **b** The unit cell volume as a function of the composition, x , for the ternary solid solution

$\text{Mg}_x\text{Nb}_{1-x}\text{O}$. The dashed line (between literature values of $V(\text{MgO})$ and $V(\text{NbO})$ open circles) indicates Vegard's law. The enlargement shows a linear correlation between the observed unit cell volume and the composition of the ternary phase

content in the ternary solid solution increases when the sample is heated and cycled with hydrogen, especially during the first four cycles, and apparently reaches a maximum. The composition after eight hydrogen release and uptake cycles is $\text{Mg}_{0.58}\text{Nb}_{0.42}\text{O}$.

The unit cell volume is plotted as a function of the composition of the solid solution $\text{Mg}_x\text{Nb}_{1-x}\text{O}$, in Fig. 16b revealing a positive deviation from Vegard's law [104]. Furthermore, the enlargement in Fig. 16b reveals a linear correlation between the unit cell volume and the composition of $\text{Mg}_x\text{Nb}_{1-x}\text{O}$ in the range $\sim 0.2 < x < \sim 0.6$. The significant volume expansion observed for $\text{Mg}_x\text{Nb}_{1-x}\text{O}$ as compared to the two binary oxides, MgO and NbO , may contribute to the prolific properties of Nb_2O_5 used as additive in MgH_2 for the release and uptake of hydrogen. Formation of $\text{Mg}_x\text{Nb}_{1-x}\text{O}$ is expected to form cracks in the otherwise dense surface layer of magnesium oxide. The increased number of diffusion pathways through the MgO layer may significantly enhance the kinetics for hydrogen release and uptake in Mg/MgH_2 [99].

4.10 Mechanisms for the catalytic enhancement of properties

As described above, in pure Mg the rate-limiting step for absorption differs from that for desorption.

The absorption process is best described by a three-dimensional diffusion-controlled contracting volume model. Therefore, to enhance hydrogen absorption either the diffusion distances have to be minimised or hydrogen diffusion through an MgH_2 layer optimised. Both in principle can be obtained by ball milling or other mechanical processes as described above. These methods reduce both particle size and grain size. In the case of particle size reduction, the diffusion distances are reduced which directly lead to an enhanced hydrogen uptake [91]. In the case of grain size reduction, a huge number of additional grain boundaries are introduced into the system. These grain boundaries have a lower packing density than the MgH_2 lattice and therefore can act as hydrogen diffusion pathways which should also help to overcome the bottleneck of slow hydrogen diffusion through the blocking MgH_2 layer. However, measurements clearly indicate that the grain size increases significantly in pure nanocrystalline Mg/MgH_2 upon cycling and/or annealing at the working temperature of 300 °C [97, 105].

In contrast, samples with transition metal oxide additions show a much smaller increase in grain size which seems to stop at a grain size around 80 nm after long-term cycling [11]. This finding, that in the presence of transition metal oxides the nanostructure is stabilised, has clearly been confirmed by small-angle scattering measurements performed by Pranzas et al. [106, 107]. In addition to these

findings which by themselves could explain the enhanced hydrogen absorption in transition metal-doped MgH_2 , measurements of Corey et al. [108] show that the hydrogen mobility is significantly increased in Nb_2O_5 -doped MgH_2 . In very good agreement to that, Borgschulte et al. [41] find a slightly destabilised phase MgH_{2-8} in Nb_2O_5 -doped MgH_2 which is formed prior to MgH_2 upon hydrogenation and could correlate the amount of this sub-stoichiometric MgH_{2-8} phase with the amount of the used transition metal oxide additive.

According to Barkhordarian et al. [42], the hydrogen desorption can be fitted best by

- Assuming a surface reaction limited process in case of small additive contents and short milling times;
- Applying a contracting volume model with two-dimensional growth and constant interface velocity in case of prolonged ball milling and catalyst contents of more than 1 mol % Nb_2O_5 .

Obviously, a shift in the rate-limiting steps from surface reaction towards a two-dimensional growth of the Mg phase with constant interface velocity occurs. During ball milling, it is observed that particle size of the material to be ground decreases considerably. Hence, the surface area increases and the surface reaction is no longer the limiting process.

Since this is also observed if the amount of transition metal oxide additives is increased, there are two possible interpretations:

- either the transition metal oxides as hard materials help in the ball milling process to refine the MgH_2 particles
- or the transition metal oxides (or the Mg-Nb-O_x products formed during the heating and cycling) themselves have a direct influence on the surface reaction, the chemisorption process or the recombination of the hydrogen molecules.

Indeed, it has been shown that the presence of transition metal oxides during ball milling helps to scale down the particle sizes of the MgH_2 [106]. Nevertheless, Borgschulte et al. [109] found a catalytic effect of niobium oxide for hydrogen dissociation with the lowest activation energy for the highest oxygen content: Nb_2O_5 . In their study, pure Nb did not display any catalytic effect.

If for desorption the chemisorption is such a crucial step which has to be overcome, one might ask the question why not just use a well-known catalyst like Ni instead of niobium oxide. Experiments performed on ball-milled MgH_2 samples with Ni and Nb_2O_5 , respectively, performed by Hanada et al. [110] showed that Ni indeed shows a very beneficial effect on MgH_2 desorption as well, however, during cycling desorption properties worsen significantly.

4.11 Future prospects

In this paper, different techniques to synthesise nanostructured magnesium were reviewed. It is clear that materials synthesised by various techniques share common features and there is also some important differences between them. Moreover, depending on the synthesis parameters a single technique can produce a drastically different end product. A familiar example is mechanical alloying where the ball-to-powder ratio, milling time and intensity can result in compounds that have very different hydrogen storage properties. Thus, when comparing synthesis techniques or the same technique in different conditions, it is crucial to also know the synthesis parameters.

This review also reveals that, under the usual hydrogenation/dehydrogenation conditions, magnesium-based materials are in fact dynamic systems. This means that the synthesised material will most likely change its properties after one or many hydrogenation/dehydrogenation cycles. This is mainly due to the high temperature required to perform hydrogenation which results in an important species diffusion and grain growth. Also, the simple act of hydrogen going in and out of the structure could lead to a change of crystal structure. This should be taken into account when new materials are designed.

It was shown that hydrogenation/dehydrogenation kinetics could be dramatically improved by the use of appropriate catalysts. In terms of suitable hydrogen storage materials, the kinetics is no longer an insurmountable problem. However, as hydrogenation/dehydrogenation is associated with a large heat of reaction, to use these materials in real situations, the big challenge will be to improve heat transfer. The engineering side of the solution of this problem is evident, but we think that material development should also play a role. We hope that in the future heat transfer will be considered as a key parameter for the scientist developing new materials.

We firmly believe that more fundamental understanding of the effect of nanocrystallinity, catalyst addition and chemical modification is needed. In particular, novel schemes such as nanoconfinement and HDDR process should be investigated further.

As presently reviewed, the thermodynamic properties of the Mg–H system can be destabilised by alloying Mg with other metals, however, at the expense of the storage capacity. The mechanical modifications of Mg/MgH₂ (with or without additives) showed impressive kinetic improvements and almost no thermodynamic changes.

The destabilisation of the Mg–H thermodynamics has been proven experimentally by nanoconfinement although to a limited extent. Small MgH₂ nanoconfined particles show an important decrease in the reaction enthalpy ($-\Delta H_f = 63.8$ kJ/mol for 3 nm particles) [25], but this is

counteracted by a shift in the change of entropy. Therefore, these thermodynamic changes correspond to a limited decrease in the equilibrium temperature at 1 bar by 11 °C, as compared to bulk MgH₂.

The theoretical investigations suggest that a significant decrease in the energy of desorption might occur for ultra-small cluster <10 Mg atoms. However, the synthesis and stabilisation against coalescence of such small Mg clusters remains a real experimental challenge.

Most of the reviewed approaches have a significant positive impact on the improvement of the hydrogen absorption/desorption kinetics. However, if there is a general agreement that these strategies are effective, an wide variation in experimental isothermal kinetic data was recently shown by a round robin test realised on the same ball-milled MgH₂ material [111]. This points out a need for a collective effort to understand the effect of different experimental parameters (driving force, additives, etc) on the interpretation of the recorded data.

All efforts to downscale the Mg/MgH₂ particle/crystallite size to the nanometre range are extremely positive in improving the kinetics of the reaction with hydrogen. However, the main experimental issue is to preserve the initial nanostructure during extensive cycling at high temperature. The use of nanoconfinement may help to prevent the sintering or recrystallisation of grains during cycling.

The use of additives is undoubtedly a big improvement of the reaction kinetics. Despite an important scientific effort using extended experimental facilities, a clear description of the mechanism of the catalytic activities is still missing for each of the additives used. Even whether the effect is properly catalytic or not is not established for all additives. Some additives are known to decompose, reduce or form more complex compounds with Mg upon cycling and are therefore not true catalysts. An understanding of the mechanisms by which additives effectively change the kinetics of the Mg–H reaction may help guide the development of even more effective additives.

The present special issue contains two other closely related papers which could be of interest for the readers entitled “Mg-based Compounds for Hydrogen and Energy Storage” [112] and “Integrated with FC H storage systems utilising magnesium hydride: experimental Studies and modelling” [113].

Acknowledgments This work is a part of the activities within IEA Task 32 Hydrogen-based Energy Storage. We are grateful for the task coordinator Dr. Michael Hirscher and all the experts from the Task 32 for the fruitful collaboration.

References

1. M. Paskevicius, D.A. Sheppard, C.E. Buckley, Thermodynamic changes in mechanochemically synthesized magnesium hydride nanoparticles. *J. Am. Chem. Soc.* **132**(14), 5077–5083 (2010)

2. J.F. Stampfer, C.E. Holley, J.F. Suttle, The magnesium-hydrogen system 1–3. *J. Am. Chem. Soc.* **82**(14), 3504–3508 (1960)
3. P. Chen, M. Zhu, Recent progress in hydrogen storage. *Mater. Today* **11**(12), 36–43 (2008)
4. C. Zlotea, M. Sahlberg, S. Özbilen, P. Moretto, Y. Andersson, Hydrogen desorption studies of the $\text{Mg}_{24}\text{Y}_5\text{-H}$ system: formation of Mg tubes, kinetics and cycling effects. *Acta Mater.* **56**(11), 2421–2428 (2008)
5. T.K. Nielsen, K. Manickam, M. Hirscher, F. Besenbacher, T.R. Jensen, Confinement of MgH_2 nanoclusters within nanoporous aerogel scaffold materials. *ACS Nano* **3**(11), 3521–3528 (2009)
6. A.F. Gross, C.C. Ahn, S.L. Van Atta, P. Liu, J.J. Vajo, Fabrication and hydrogen sorption behaviour of nanoparticulate MgH_2 incorporated in a porous carbon host. *Nanotechnology* **20**(20), 204005 (2009)
7. S. Zhang, A.F. Gross, S.L. Van Atta, M. Lopez, P. Liu, C.C. Ahn, J.J. Vajo, C.M. Jensen, The synthesis and hydrogen storage properties of a MgH_2 incorporated carbon aerogel scaffold. *Nanotechnology* **20**(20), 204027 (2009)
8. J. Huot, D.B. Ravnsbæk, J. Zhang, F. Cuevas, M. Latroche, T.R. Jensen, Mechanochemical synthesis of hydrogen storage materials. *Prog. Mater. Sci.* **58**(1), 30–75 (2013)
9. C.J. Webb, A review of catalyst-enhanced magnesium hydride as a hydrogen storage material. *J. Phys. Chem. Solids* **84**, 96–106 (2015)
10. R.A. Varin, L. Zbroniec, M. Polanski, J. Bystrzycki, A review of recent advances on the effects of microstructural refinement and nano-catalytic additives on the hydrogen storage properties of metal and complex hydrides. *Energies* **4**(1), 1–25 (2010)
11. M. Dornheim, S. Doppiu, G. Barkhordarian, U. Boesenberg, T. Klassen, O. Gutfleisch, R. Bormann, Hydrogen storage in magnesium-based hydrides and hydride composites. *Scr. Mater.* **56**(10), 841–846 (2007)
12. F. Cheng, Z. Tao, J. Liang, J. Chen, Efficient hydrogen storage with the combination of lightweight Mg/MgH_2 and nanostructures. *Chem. Commun.* **48**(59), 7334–7343 (2012)
13. C. Zlotea, M. Latroche, Role of nanoconfinement on hydrogen sorption properties of metal nanoparticles hybrids. *Colloids Surf. A* **439**, 117–130 (2013)
14. P. Vajeeston, P. Ravindran, B.C. Hauback, H. Fjellvåg, A. Kjekshus, S. Furuseth, M. Hanfland, Structural stability and pressure-induced phase transitions in MgH_2 . *Phys. Rev. B* **73**(22), 224102 (2006)
15. J. Huot, I. Swainson, R. Schulz, Phase transformation in magnesium hydride induced by ball milling. *Annales de Chimie* **31**(1), 135–144 (2006)
16. W.H. Zachariasen, C.E. Holley, J.F. Stamper Jr, Neutron diffraction study of magnesium deuteride. *Acta Crystallogr.* **16**(5), 352–353 (1963)
17. M. Bortz, B. Bertheville, G. Böttger, K. Yvon, Structure of the high pressure phase $\gamma\text{-MgH}_2$ by neutron powder diffraction. *J. Alloys Compd.* **287**(1–2), L4–L6 (1999)
18. P. Vajeeston, P. Ravindran, A. Kjekshus, H. Fjellvåg, Pressure-Induced Structural Transitions in MgH_2 . *Phys Rev Lett* **89**(17), 175506 (2002)
19. P. Vajeeston, P. Ravindran, H. Fjellvåg, Chemical Bonding in Hydrides, in *Advances in Chemistry Research*, ed. by J.C. Taylor (Nova Science Publishers, New York City, 2011), pp. 177–200
20. D. Moser, G. Baldissin, D.J. Bull, D.J. Riley, I. Morrison, D.K. Ross, W.A. Oates, D. Noréus, The pressure–temperature phase diagram of MgH_2 and isotopic substitution. *J. Phys.: Condens. Matter* **23**(30), 305403 (2011)
21. M. Wagemans, J.H. van Lenthe, P.E. de Jongh, A.J. van Dillen, K.P. de Jong, Hydrogen Storage in Magnesium clusters: quantum chemical study. *J. Am. Chem. Soc.* **127**, 16675–16680 (2005)
22. S. Cheung, W.Q. Deng, A.C. van Duin, W.A. Goddard 3rd, ReaxFF(MgH) reactive force field for magnesium hydride systems. *J. Phys. Chem. A* **109**(5), 851–859 (2005)
23. V. Bérubé, G. Radtke, M. Dresselhaus, G. Chen, Size effects on the hydrogen storage properties of nanostructured metal hydrides: a review. *Int. J. Energy Res.* **31**(6–7), 637–663 (2007)
24. K.C. Kim, B. Dai, J. Karl Johnson, D.S. Sholl, Assessing nanoparticle size effects on metal hydride thermodynamics using the Wulff construction. *Nanotechnology* **20**(20), 204001 (2009)
25. Z. Zhao-Karger, J. Hu, A. Roth, D. Wang, C. Kubel, W. Lohstroh, M. Fichtner, Altered thermodynamic and kinetic properties of MgH_2 infiltrated in microporous scaffold. *Chem. Commun.* **46**(44), 8353–8355 (2010)
26. Z. Wu, M.D. Allendorf, J.C. Grossman, Quantum monte carlo simulation of nanoscale MgH_2 cluster thermodynamics. *J. Am. Chem. Soc.* **131**(39), 13918–13919 (2009)
27. A.C. Buckley, D.J. Carter, D.A. Sheppard, C.E. Buckley, Density functional theory calculations of magnesium hydride: a comparison of bulk and nanoparticle thermodynamics. *J. Phys. Chem. C* **116**(33), 17985–17990 (2012)
28. J.J. Vajo, F. Mertens, C.C. Ahn, R.C. Bowman, B. Fultz, Altering hydrogen storage properties by hydride destabilization through alloy formation: LiH and MgH_2 destabilized with Si. *J. Phys. Chem. B* **108**(37), 13977–13983 (2004)
29. J.J. Vajo, G.L. Olson, Hydrogen storage in destabilized chemical systems. *Scr. Mater.* **56**(10), 829–834 (2007)
30. J.C. Crivello, T. Nobuki, S. Kato, M. Abe, T. Kuji, Hydrogen absorption properties of the $\text{-Mg}_{17}\text{Al}_{12}$ phase and its Al-rich domains. *J. Alloys Compd.* **446–447**, 157–161 (2007)
31. Q.A. Zhang, H.Y. Wu, Hydriding behavior of $\text{Mg}_{17}\text{Al}_{12}$ compound. *Mater. Chem. Phys.* **94**(1), 69–72 (2005)
32. S. Bouaricha, J.P. Dodelet, D. Guay, J. Huot, S. Boily, R. Schulz, Hydriding behavior of Mg–Al and leached Mg–Al compounds prepared by high-energy ball-milling. *J. Alloys Compd.* **297**, 282–293 (2000)
33. A. Andreasen, M.B. Sørensen, R. Burkarl, B. Möller, A.M. Molenbroek, A.S. Pedersen, J.W. Andreasen, M.M. Nielsen, T.R. Jensen, Interaction of hydrogen with an Mg–Al alloy. *J. Alloys Compd.* **404–406**, 323–326 (2005)
34. K. Klyukin, M.G. Shelyapina, D. Fruchart, Hydrogen induced phase transition in magnesium: An Ab initio study. *J. Alloys Compd.* **580**, S10–S12 (2013)
35. X.H. Tan, L.Y. Wang, C.M.B. Holt, B. Zahiri, M.H. Eikerling, D. Mitlin, Body centered cubic magnesium niobium hydride with facile room temperature absorption and four weight percent reversible capacity. *Phys. Chem. Chem. Phys.* **14**(31), 10904–10909 (2012)
36. L.P.A. Mooij, A. Baldi, C. Boelsma, K. Shen, M. Wagemaker, Y. Pivak, H. Schreuders, R. Griessen, B. Dam, Interface energy controlled thermodynamics of nanoscale metal hydrides. *Adv. Energy Mat.* **1**(5), 754–758 (2011)
37. D. Korablov, F. Besenbacher, T.R. Jensen, Ternary compounds in the magnesium–titanium hydrogen storage system. *Int. J. Hydrogen Energy* **39**(18), 9700–9708 (2014)
38. P. Kalisvaart, B. Shalchi-Amirkhiz, R. Zahiri, B. Zahiri, X. Tan, M. Danaie, G. Botton, D. Mitlin, Thermodynamically destabilized hydride formation in “bulk” Mg–AlTi multilayers for hydrogen storage. *Phys. Chem. Chem. Phys.* **15**(39), 16432–16436 (2013)
39. C. Zhou, Z.Z. Fang, J. Lu, X. Luo, C. Ren, P. Fan, Y. Ren, X. Zhang, Thermodynamic destabilization of magnesium hydride using Mg-based solid solution alloys. *J. Phys. Chem. C* **118**(22), 11526–11535 (2014)

40. M. Dornheim, T. Klassen, *High Temperature Hydrides. Encyclopedia of Electrochemical Power Sources* (Elsevier, Amsterdam, 2009), pp. 459–472
41. A. Borgschulte, U. Bösenberg, G. Barkhordarian, M. Dornheim, R. Bormann, Enhanced hydrogen sorption kinetics of magnesium by destabilized MgH_{2-8} . *Catal. Today* **120**, 262–269 (2007)
42. G. Barkhordarian, T. Klassen, R. Bormann, Kinetic investigation of the effect of milling time on the hydrogen sorption reaction of magnesium catalyzed with different Nb_2O_5 contents. *J. Alloys Compd.* **407**, 249–255 (2006)
43. H.M. Mintz, Y. Zeiri, Review: hydriding kinetics of powders. *J. Alloys Compd.* **216**, 159–175 (1994)
44. E. Evard, I. Gabis, V.A. Yartys, Kinetics of hydrogen evolution from MgH_2 : experimental studies, mechanism and modelling. *Int. J. Hydrogen Energy* **35**(17), 9060–9069 (2010)
45. J. Huot, G. Liang, R. Schulz, Mechanically alloyed metal hydride systems. *Appl. Phys.* **72**(2), 187–195 (2001)
46. P. Kuziora, M. Wyszynska, M. Polanski, J. Bystrzycki, Why the ball to powder ratio (BPR) is insufficient for describing the mechanical ball milling process. *Int. J. Hydrogen Energy* **39**(18), 9883–9887 (2014)
47. R.V. Denys, A.B. Riabov, J.P. Maehlen, M.V. Lototsky, J.K. Solberg, V.A. Yartys, In situ synchrotron X-ray diffraction studies of hydrogen desorption and absorption properties of Mg and Mg–Mm–Ni after reactive ball milling in hydrogen. *Acta Mater.* **57**(13), 3989–4000 (2009)
48. V. Skripnyuk, E. Rabkin, Y. Estrin, R. Lapovok, The effect of ball milling and equal channel angular pressing on hydrogen absorption/desorption properties of Mg–4.95 wt% Zn–0.71 wt% Zr (ZK60) alloy. *Acta Mater.* **52**(2), 405–414 (2004)
49. V. Skripnyuk, E. Buchman, E. Rabkin, Y. Estrin, M. Popov, S. Jorgensen, The effect of equal channel angular pressing on hydrogen storage properties of a eutectic Mg–Ni alloy. *J. Alloys Compd.* **436**, 99–106 (2007)
50. V.M. Skripnyuk, E. Rabkin, Y. Estrin, R. Lapovok, Improving hydrogen storage properties of magnesium based alloys by equal channel angular pressing. *Int. J. Hydrogen Energy* **34**(15), 6320–6324 (2009)
51. V.M. Skripnyuk, E. Rabkin, L.A. Bendersky, A. Magrez, E. Carreño-Morelli, Y. Estrin, Hydrogen storage properties of as-synthesized and severely deformed magnesium—multiwall carbon nanotubes composite. *Int. J. Hydrogen Energy* **35**(11), 5471–5478 (2010)
52. S. Løken, J.K. Solberg, J.P. Maehlen, R.V. Denys, M.V. Lototsky, B.P. Tarasov, V.A. Yartys, Nanostructured Mg–Mm–Ni hydrogen storage alloy: structure-properties relationship. *J. Alloys Compd.* **446–447**, 114–120 (2007)
53. Á. Révész, M. Gajdics, L.K. Varga, G. Krállics, L. Péter, T. Spassov, Hydrogen storage of nanocrystalline Mg–Ni alloy processed by equal-channel angular pressing and cold rolling. *Int. J. Hydrogen Energy* **39**(18), 9911–9917 (2014)
54. M. Krystian, M.J. Zehetbauer, H. Kropik, B. Mingler, G. Krexner, Hydrogen storage properties of bulk nanostructured ZK60 Mg alloy processed by equal channel angular pressing. *J. Alloys Compd.* **509**(Suppl 1), S449–S455 (2011)
55. A.M. Jorge Jr, G.F. de Lima, M.R. Martins Triques, W.J. Botta, C.S. Kiminami, R.P. Nogueira, A.R. Yavari, T.G. Langdon, Correlation between hydrogen storage properties and textures induced in magnesium through ECAP and cold rolling. *Int. J. Hydrogen Energy* **39**(8), 3810–3821 (2014)
56. Y. Wu, W. Han, S.X. Zhou, M.V. Lototsky, J.K. Solberg, V.A. Yartys, Microstructure and hydrogenation behavior of ball-milled and melt-spun Mg–10Ni–2 Mm alloys. *J. Alloys Compd.* **466**(1–2), 176–181 (2008)
57. Y. Wu, M.V. Lototsky, J.K. Solberg, V.A. Yartys, W. Han, S.X. Zhou, Microstructure and novel hydrogen storage properties of melt-spun Mg–Ni–Mm alloys. *J. Alloys Compd.* **477**(1–2), 262–266 (2009)
58. Y. Wu, J.K. Solberg, V.A. Yartys, The effect of solidification rate on microstructural evolution of a melt-spun Mg–20Ni–8 Mm hydrogen storage alloy. *J. Alloys Compd.* **446–447**, 178–182 (2007)
59. R.V. Denys, A.A. Poletaev, J.K. Solberg, B.P. Tarasov, V.A. Yartys, LaMg_{11} with a giant unit cell synthesized by hydrogen metallurgy: crystal structure and hydrogenation behavior. *Acta Mater.* **58**(7), 2510–2519 (2010)
60. A.A. Poletaev, R.V. Denys, J.K. Solberg, B.P. Tarasov, V.A. Yartys, Microstructural optimization of LaMg_{12} alloy for hydrogen storage. *J. Alloys Compd.* **509**, S633–S639 (2011)
61. A.A. Poletaev, R.V. Denys, J.P. Maehlen, J.K. Solberg, B.P. Tarasov, V.A. Yartys, Nanostructured rapidly solidified $\text{LaMg}_{11}\text{Ni}$ alloy: microstructure, crystal structure and hydrogenation properties. *Int. J. Hydrogen Energy* **37**(4), 3548–3557 (2012)
62. P.E. de Jongh, P. Adelhelm, Nanosizing and nanoconfinement: new strategies towards meeting hydrogen storage goals. *ChemSusChem* **3**(12), 1332–1348 (2010)
63. T.K. Nielsen, F. Besenbacher, T.R. Jensen, Nanoconfined hydrides for energy storage. *Nanoscale* **3**(5), 2086–2098 (2011)
64. C. Zlotea, F. Cuevas, J. Andrieux, C. Matei Ghimbeu, E. Leroy, E. Léonel, S. Sengmany, C. Vix-Guterl, R. Gadiou, T. Martens, M. Latroche, Tunable synthesis of (Mg–Ni)-based hydrides nanoconfined in templated carbon studied by in situ synchrotron diffraction. *Nano Energy* **2**(1), 12–20 (2013)
65. P.E. de Jongh, R.W.P. Wagemans, T.M. Eggenhuisen, B.S. Dauvillier, P.B. Radstake, J.D. Meeldijk, J.W. Geus, K.P.D. Jong, The preparation of carbon-supported magnesium nanoparticles using melt infiltration. *Chem. Mater.* **19**(24), 6052–6057 (2007)
66. P. Javadian, C. Zlotea, C.M. Ghimbeu, M. Latroche, T.R. Jensen, Hydrogen storage properties of nanoconfined $\text{LiBH}_4\text{--Mg}_2\text{NiH}_4$ reactive hydride composites. *J. Phys. Chem. C* **119**(11), 5819–5826 (2015)
67. Y.S. Au, M.K. Obbink, S. Srinivasan, P.C.M.M. Magusin, K.P. de Jong, P.E. de Jongh, The size dependence of hydrogen mobility and sorption kinetics for carbon-supported MgH_2 particles. *Adv. Funct. Mater.* **24**(23), 3604–3611 (2014)
68. C. Zlotea, Y. Oumellal, S.-J. Hwang, C.M. Ghimbeu, P.E. de Jongh, M. Latroche, Ultrasmall MgH_2 Nanoparticles embedded in an ordered microporous carbon exhibiting rapid hydrogen sorption kinetics. *J. Phys. Chem. C* **119**(32), 18091–18098 (2015)
69. R. Bogerd, P. Adelhelm, J.H. Meeldijk, K.P. de Jong, P.E. de Jongh, The structural characterization and H_2 sorption properties of carbon-supported $\text{Mg}_{1-x}\text{Ni}_x$ nanocrystallites. *Nanotechnology* **20**(20), 204019 (2009)
70. G. Siviero, V. Bello, G. Mattei, P. Mazzoldi, G. Battaglin, N. Bazzanella, R. Checchetto, A. Miotello, Structural evolution of Pd-capped Mg thin films under H_2 absorption and desorption cycles. *Int. J. Hydrogen Energy* **34**(11), 4817–4826 (2009)
71. C.E. Buckley, H.K. Birnbaum, J.S. Lin, S. Spooner, D. Bellmann, P. Staron, T.J. Udovic, E. Hollar, Characterization of H defects in the aluminium-hydrogen system using small-angle scattering techniques. *J. Appl. Crystallogr.* **34**(2), 119–129 (2001)
72. D. Milcius, J. Grbović-Novaković, R. Zostautienė, M. Lelis, D. Girdzevicius, M. Urbonavicius, Combined XRD and XPS analysis of ex situ and in situ plasma hydrogenated magnetron sputtered Mg films. *J. Alloys Compd.* **647**, 790–796 (2015)

73. R. Gremaud, C.P. Broedersz, D.M. Borsa, A. Borgschulte, P. Mauron, H. Schreuders, J.H. Rector, B. Dam, R. Griessen, Hydrogenography: an optical combinatorial method to find new light-weight hydrogen-storage materials. *Adv. Mater.* **19**(19), 2813–2817 (2007)
74. D.M. Borsa, R. Gremaud, A. Baldi, H. Schreuders, J.H. Rector, B. Kooi, P. Vermeulen, P.H.L. Notten, B. Dam, R. Griessen, Structural, optical, and electrical properties of $\text{Mg}_y\text{Ti}_{1-y}\text{H}_x$ thin films. *Phys. Rev. B* **75**(20), 205408 (2007)
75. A. Baldi, R. Gremaud, D. Borsa, C. Balde, A. Vandereerden, G. Kruijtzter, P. Dejongh, B. Dam, R. Griessen, Nanoscale composition modulations in $\text{Mg}_y\text{Ti}_{1-y}\text{H}_x$ thin film alloys for hydrogen storage. *Int. J. Hydrogen Energy* **34**(3), 1450–1457 (2009)
76. K. Asano, R.J. Westerwaal, A. Anastasopol, L.P.A. Mooij, C. Boelsma, P. Ngene, H. Schreuders, S.W.H. Eijt, B. Dam, Destabilization of Mg hydride by self-organized nanoclusters in the immiscible Mg–Ti system. *J. Phys. Chem. C* **119**(22), 12157–12164 (2015)
77. K. Asano, H. Kim, K. Sakaki, K. Page, S. Hayashi, Y. Nakamura, E. Akiba, Synthesis and structural study of Ti-rich Mg–Ti hydrides. *J. Alloys Compd.* **593**, 132–136 (2014)
78. L. Mooij, T. Perkisas, G. Pálsson, H. Schreuders, M. Wolff, B. Hjörvarsson, S. Bals, B. Dam, The effect of microstructure on the hydrogenation of Mg/Fe thin film multilayers. *Int. J. Hydrogen Energy* **39**(30), 17092–17103 (2014)
79. A. Baldi, M. Gonzalez-Silveira, V. Palmisano, B. Dam, R. Griessen, Destabilization of the Mg–H system through elastic constraints. *Phys. Rev. Lett.* **102**(22), 226102 (2009)
80. C.J. Chung, S.-C. Lee, J.R. Groves, E.N. Brower, R. Sinclair, Clemens BM (2012) Interfacial Alloy Hydride Destabilization in Mg/Pd Thin Films. *Phys Rev Lett.* **108**(10), 106102 (2012)
81. L. Mooij, B. Dam, Hysteresis and the role of nucleation and growth in the hydrogenation of Mg nanolayers. *Phys. Chem. Chem. Phys.* **15**(8), 2782 (2013)
82. M. Lototsky, J.M. Sibanyoni, R.V. Denys, M. Williams, B.G. Pollet, V.A. Yartys, Magnesium–carbon hydrogen storage hybrid materials produced by reactive ball milling in hydrogen. *Carbon* **57**, 146–160 (2013)
83. K. Alsabawi, T.A. Webb, E.M. Gray, C.J. Webb, Effect of C_{60} additive on magnesium hydride for hydrogen storage. *Int. J. Hydrogen Energy* **40**(33), 10508–10515 (2015)
84. D. Korablov, J. Ångström, M.B. Ley, M. Sahlberg, F. Besenbacher, T.R. Jensen, Activation effects during hydrogen release and uptake of MgH_2 . *Int. J. Hydrogen Energy* **39**(18), 9888–9892 (2014)
85. M.V. Lototsky, R.V. Denys, V.A. Yartys, Combustion-type hydrogenation of nanostructured Mg-based composites for hydrogen storage. *Int. J. Energy Res.* **33**(13), 1114–1125 (2009)
86. G. Barkhordarian, T. Klassen, R. Bormann, Fast hydrogen sorption kinetics of nanocrystalline Mg using Nb_2O_5 as catalyst. *Scr. Mater.* **49**(3), 213–217 (2003)
87. M.P. Pitt, M. Paskevicius, C.J. Webb, D.A. Sheppard, C.E. Buckley, E.M. Gray, The synthesis of nanoscopic Ti based alloys and their effects on the MgH_2 system compared with the $\text{MgH}_2 + 0.01\text{Nb}_2\text{O}_5$ benchmark. *Int. J. Hydrogen Energy* **37**(5), 4227–4237 (2012)
88. J. Lu, Y.J. Choi, Z.Z. Fang, H.Y. Sohn, E. Ronnebro, Hydrogen storage properties of nanosized $\text{MgH}_2\text{-}0.1\text{TiH}_2$ prepared by ultrahigh-energy-high-pressure milling. *J. Am. Chem. Soc.* **131**(43), 15843–15852 (2009)
89. X. Zhu, L. Pei, Z. Zhao, B. Liu, S. Han, R. Wang, The catalysis mechanism of La hydrides on hydrogen storage properties of MgH_2 in $\text{MgH}_2 + x \text{ wt\% LaH}_3$ ($x = 0, 10, 20$ and 30) composites. *J. Alloys Compd.* **577**, 64–69 (2013)
90. A. Zaluska, L. Zaluski, J.O. Ström-Olsen, Nanocrystalline magnesium for hydrogen storage. *J. Alloys Compd.* **288**(1–2), 217–225 (1999)
91. M. Dornheim, N. Eigen, G. Barkhordarian, T. Klassen, R. Bormann, Tailoring hydrogen storage materials towards application. *Adv. Eng. Mater.* **8**(5), 377–385 (2006)
92. K.F. Aguey-Zinsou, T. Nicolaisen, J.R. Ares Fernandez, T. Klassen, R. Bormann, Effect of nanosized oxides on MgH_2 (de)hydriding kinetics. *J. Alloys Compd.* **434–435**, 738–742 (2007)
93. W. Oelerich, T. Klassen, R. Bormann, Metal oxides as catalysts for improved hydrogen sorption in nanocrystalline Mg-based materials. *J. Alloys Compd.* **315**(1–2), 237–242 (2001)
94. G. Barkhordarian, T. Klassen, R. Bormann, Effect of Nb_2O_5 content on hydrogen reaction kinetics of Mg. *J. Alloys Compd.* **364**(1–2), 242–246 (2004)
95. G. Barkhordarian, T. Klassen, R. Bormann, Catalytic mechanism of transition-metal compounds on Mg hydrogen sorption reaction. *J. Phys. Chem. B* **110**(22), 11020–11024 (2006)
96. F. Dolci, M.D. Chio, M. Baricco, E. Giamello, Niobium pentoxide as promoter in the mixed $\text{MgH}_2/\text{Nb}_2\text{O}_5$ system for hydrogen storage: a multitechnique investigation of the H_2 uptake. *J. Mater. Sci.* **42**(17), 7180–7185 (2007)
97. O. Friedrichs, F. Aguey-Zinsou, J.R. Ares Fernandez, J.C. Sanchez-Lopez, A. Justo, T. Klassen, R. Bormann, A. Fernandez, MgH_2 with Nb_2O_5 as additive for hydrogen storage: chemical, structural and kinetic behaviour with heating. *Acta Mater.* **54**, 105–110 (2006)
98. O. Friedrichs, D. Martinez-Martinez, G. Guilera, J.C. Sanchez-Lopez, A. Fernandez, In situ energy-dispersive XAS and XRD study of the superior hydrogen storage system $\text{MgH}_2/\text{Nb}_2\text{O}_5$. *J. Phys. Chem. C* **111**(28), 10700–10706 (2007)
99. O. Friedrichs, J.C. Sánchez-López, C. López-Cartes, T. Klassen, R. Bormann, A. Fernández, Nb_2O_5 “Pathway effect” on hydrogen sorption in Mg. *J. Phys. Chem. B* **110**(15), 7845–7850 (2006)
100. T.R. Jensen, T.K. Nielsen, Y. Filinchuk, J.-E. Jorgensen, Y. Cerenius, E.M. Gray, C.J. Webb, Versatile in situ powder X-ray diffraction cells for solid-gas investigations. *J. Appl. Crystallogr.* **43**(6), 1456–1463 (2010)
101. B.R.S. Hansen, K.T. Møller, M. Paskevicius, A.-C. Dippel, P. Walter, C.J. Webb, C. Pistidda, N. Bergemann, M. Dornheim, T. Klassen, J.-E. Jørgensen, T.R. Jensen, In situ X-ray diffraction environments for high-pressure reactions. *J. Appl. Crystallogr.* **48**(4), 1234–1241 (2015)
102. T.K. Nielsen, T.R. Jensen, $\text{MgH}_2\text{-Nb}_2\text{O}_5$ investigated by in situ synchrotron X-ray diffraction. *Int. J. Hydrogen Energy* **37**(18), 13409–13416 (2012)
103. A. Aurora, M.R. Mancini, D.M. Gattia, A. Montone, L. Pilloni, E. Todini, M.V. Antisari, Microstructural and kinetic investigation of hydrogen sorption reaction of $\text{MgH}_2/\text{Nb}_2\text{O}_5$ nanopowders. *Mater. Manuf. Process.* **24**(10–11), 1058–1063 (2009)
104. L. Vegard, Die Konstitution der Mischkristalle und die Raumfüllung der Atome. *Z. Phys.* **5**(1), 17–26 (1921)
105. P.-A. Huhn, M. Dornheim, T. Klassen, R. Bormann, Thermal stability of nanocrystalline magnesium for hydrogen storage. *J. Alloys Compd.* **404–406**, 499–502 (2005)
106. P.K. Pranzas, M. Dornheim, D. Bellmann, F. Aguey-Zinsou, T. Klassen, A. Schreyer, SANS/USANS investigations of nanocrystalline MgH_2 for reversible storage of hydrogen. *Physica B* **385–386**, 630–632 (2006)
107. P.K. Pranzas, M. Dornheim, U. Bösenberg, J.R. Ares Fernandez, G. Goerigk, S. Roth, R. Gehrke, A. Schreyer, Small-angle scattering investigations of magnesium hydride used as a

- hydrogen storage material. *J. Appl. Crystallogr.* **40**, 383–387 (2007)
108. R.L. Corey, T.M. Ivancic, D.T. Shane, E.A. Carl, R.C. Bowman, J.M. Bellosta von Colbe, M. Dornheim, R. Bormann, J. Huot, R. Zidan, A.C. Stowe, M.S. Conradi, Hydrogen motion in magnesium hydride by NMR. *J. Phys. Chem. C* **112**, 19784–19790 (2008)
109. A. Borgschulte, J.H. Rector, B. Dam, R. Griessen, A. Züttel, The role of niobium oxide as a surface catalyst for hydrogen absorption. *J. Catal.* **235**, 353–358 (2005)
110. N. Hanada, T. Ichikawa, H. Fujii, Catalytic effect of Ni nanoparticle and Nb oxide on H-desorption properties in MgH_2 prepared by ball-milling. *J. Alloys Compd.* **404**, 716–719 (2005)
111. P. Moretto, C. Zlotea, F. Dolci, A. Amieiro, J.L. Bobet, A. Borgschulte, D. Chandra, H. Enoki, P. De Rango, D. Fruchart, J. Jepsen, M. Latroche, I.L. Jansa, D. Moser, S. Sartori, S.M. Wang, J.A. Zan, A Round Robin Test exercise on hydrogen absorption/desorption properties of a magnesium hydride based material. *Int. J. Hydrogen Energy* **38**(16), 6704–6717 (2013)
112. J.-C. Crivello, R.V. Denys, M. Dornheim, M. Felderhoff, D.M. Grant, J. Huot, T.R. Jensen, M. Latroche, C. Milanese, G.S. Walker, Mg-based Compounds for Hydrogen and Energy Storage. *Appl. Phys. A* This issue
113. P. de Rango, P. Marty, D. Fruchart, Integrated with FC H storage systems utilising magnesium hydride: experimental studies and modelling. *Appl. Phys. A* This issue